

Advanced SYNCOM

BUTTO

February 1963

MONTHLY PROGRESS REPORT

NASA Contract 5-2797
SSD 3119R

FACILITY FORM 808	N66-83656	
	(ACCESSION NUMBER)	
	60	NONE
	(PAGES)	(CODE)
	CR-74586	
	(NASA CR OR TMX OR AD NUMBER)	(CATEGORY)

AEROSPACE GROUP
SPACE SYSTEMS DIVISION
HUGHES AIRCRAFT COMPANY
CULVER CITY, CALIFORNIA

HUGHES

HUGHES AIRCRAFT COMPANY

AEROSPACE GROUP

SPACE SYSTEMS DIVISION

CULVER CITY, CALIFORNIA

15 March 1963

SUBJECT: Advanced Syncom Monthly Progress
Report for February 1963

TO: Mr. Alton E. Jones
Program Manager, Syncom
Goddard Space Flight Center
Code 621
Greenbelt, Maryland

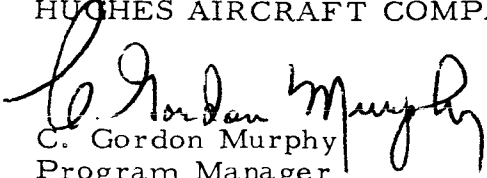
Attached are copies of the Advanced Syncom Monthly Progress Report for February 1963.

Preparations for the preliminary engineering acceptance demonstrations were completed during the report period. The phased array antenna, and its associated control circuitry, the frequency translation transponder, and multiple access transponder, a traveling-wave tube final power amplifier, and a collinear array receiving antenna were integrated into the engineering model structure. The structure was mounted on a spin fixture which permits conduct of dynamic spinning tests of the spacecraft systems.

In addition to the engineering equipment incorporated into the structure, Syncom I telemetry and command equipment were adapted to the requirements of the Syncom II equipment to permit command control and status assessment of the spinning spacecraft through RF command and telemetry links.

Demonstrations of the engineering performance were conducted on 2 March and 15 March 1963 to representatives of NASA and the Department of Defense.

HUGHES AIRCRAFT COMPANY


C. Gordon Murphy
Program Manager
Project Syncom

cc: H. E. Tetirick
Goddard Space Flight Center
Code 241.4
Greenbelt, Maryland

Advanced SYNCOM

February 1963

MONTHLY PROGRESS REPORT

•

*NASA Contract 5-2797
SSD 3119R*

AEROSPACE GROUP
SPACE SYSTEMS DIVISION
HUGHES AIRCRAFT COMPANY
CULVER CITY, CALIFORNIA

HUGHES

CONTENTS

	Page
1. INTRODUCTION	1-1
2. SYSTEM DESIGN STUDY	2-1
Communication Subsystem	2-1
System Reliability Studies	2-4
Components and Materials	2-6
3. ADVANCED TECHNOLOGICAL DEVELOPMENT	3-1
Dual-Mode Transponder	3-1
Transponder Test and Demonstration Panel	3-4
Traveling Wave Tube	3-4
Phased Array Transmitting Antenna	3-5
Collinear Array Receiving Antennas	3-14
Structure	3-23
Handling and Weight and Balance Equipment	3-27
Hot Gas Reaction Jet Control Subsystem	3-27
Apogee Engine Liaison	3-31
4. NEW TECHNOLOGY	4-1
5. PROJECT REFERENCE REPORT	5-1
6. ATTACHMENTS	6-1
Attachment 1. Syncom II Engineering Model	
Vibration Test Plan	6-1
Attachment 2. Syncom II Apogee Motor	
Tolerances	6-7

1. INTRODUCTION

Under NASA Goddard Space Flight Center Contract NAS-5-2797, Hughes Aircraft Company is conducting feasibility studies and advanced technological development for an advanced, stationary, active repeater, communication satellite.

An Initial Project Development Plan, submitted to Goddard on 15 August 1962, reported the initial system feasibility studies and delineated technical approaches, administrative plan, manpower requirements, schedule, and funding considerations appropriate for accomplishing the NASA contract objectives.

These monthly technical letter reports present the technical progress made during the reporting period, critical problems or delays encountered, and plans for the forthcoming reporting period. Separate reports of schedule status are provided through biweekly PERT reports. Monthly Financial Management reports provide the funding status.

2. SYSTEM DESIGN STUDY

COMMUNICATION SUBSYSTEM

Doppler Shift Expression from Orbital Parameters

An approximate expression has been derived for the Doppler frequency shift f_d of a signal emitted from an earth station at a frequency f_o to a near stationary satellite in terms of the Keplerian orbital elements of the spacecraft and the relative geographic location of the earth station. Results show that the instantaneous relative motion along the line of sight from earth station to satellite induces a frequency shift

$$f_d \approx \frac{-f_o V_c}{c \left[1 + \left(\frac{r}{R_e} \right)^2 - 2 \frac{r}{R_e} \cos (\Delta\lambda) \cos L_E \right]^{1/2}} + \left\{ \frac{i (1+e \cos \theta) \cos (\omega + \theta) \cos (\Delta\lambda) \sin L_E}{(1 - e^2)^{1/2}} + \left(\frac{1 - e^2}{1 + e \cos \theta} - \frac{1 + e \cos \theta}{(1 - e^2)^{1/2}} \right) \sin \Delta\lambda - \frac{e \sin \theta}{(1 - e^2)^{1/2}} \left(\frac{r}{R_e} - \cos (\Delta\lambda) \cos L_E \right) \right\} \quad [\text{cps}] \quad (2-1)$$

where

V_c = circular orbit synchronous velocity

= 10,087.5 fps

r/R_e = ratio of synchronous to earth equatorial radius

≅ 6.6

$\Delta\lambda$ = longitude difference between earth station and subsatellite point, positive for stations west of subsatellite point

$c = f_o \lambda_f$ = velocity of light $\approx 984.3 \times 10^6$ fps; λ_f = wavelength, feet

L_E = latitude of transmitting station, positive north

i = inclination of orbital plane to equatorial plane, radians, ≤ 5 degrees (0.0873 radian)

e = orbital eccentricity, ≤ 0.0873

θ = true anomaly, measured from perigee, $0 \leq \theta < 2\pi$

ω = argument of perigee, measured from ascending node to perigee point, $0 \leq \omega < 2\pi$

For example, if the radian measure of the inclination $i \approx 0.1$ degree is set equal to the eccentricity $e \approx 0.00175$, and a station at New York City ($L_E \approx 41^\circ$ N, $\lambda_E \approx 74^\circ$ W) transmits to a satellite stationed over the Atlantic Ocean (longitude = 25° W), then the maximum motion \dot{R}_{\max} along the line of sight occurs when $\theta \approx 2/5\pi$ and $\omega = \pi$, i. e.,

$$\dot{R}_{\max} \approx 17.6 \text{ fps} \quad (2-2)$$

$$\begin{aligned} f_{d\max} &= \frac{f_o}{c} 17.6 = \frac{17.6}{\lambda_f} \\ &= \frac{17.6}{0.1637} \Bigg|_{f_o = 6 \text{ kmc}} \approx 107.5 \text{ cps} \end{aligned} \quad (2-3)$$

However, most of this motion is along the geocentric radius to the spacecraft in the form of vertical velocity, the maximum rate difference along the lines of sight as seen by two earth stations to the satellite (located at opposite ends of the continuous visibility cone formed by the spacecraft and the locus of minimum station elevation lines to the satellite) will be less than 17.6 fps indicated above. The corresponding Doppler shift difference will also be less than 107.5 cps of the above example.

An estimate of the maximum Doppler difference may be obtained by expressing Equation 2-1 in terms of the half-apex angle ϕ , of the visibility cone, and the azimuth angle ψ between the meridian plane containing the spacecraft and the plane formed by the line of sight from the earth station to the spacecraft and the geocentric radius to the spacecraft (Figure 2-1).

Specifically,

$$f_d \approx \frac{f_o V_c}{c} \left[\frac{i (1 + e \cos \theta) \cos (\omega + \theta) \sin \phi \cos \psi}{(1 - e^2)^{1/2}} + \left(\frac{1 - e^2}{1 + e \cos \theta} - \frac{1 + e \cos \theta}{(1 - e^2)^{1/2}} \right) \sin \phi \sin \psi - \frac{e \sin \theta \cos \phi}{(1 - e^2)^{1/2}} \right] \quad (2-4)$$

Now, by forming the difference

$$\Delta f_d = f_{d2} - f_{d1} \quad (2-5)$$

using Equation 2-4 and neglecting terms of order e^2 or higher, the fact that

$$0 \leq \phi < 8.65^\circ = \phi_{\max} \quad (2-6)$$

is used to estimate (note: $e \approx i, \omega = \pi$)

$$\Delta f_d \Big|_{\phi_2 = \phi_1 = \phi_{\max}} \approx \frac{f_o V_c e}{c} \cos \theta \sin \phi_{\max} (\cos \psi_2 - \cos \psi_1 + \sin \psi_2 - \sin \psi_1) \quad (2-7)$$

From Equation 2-7 it is estimated (at $\theta = 0$)

$$\begin{aligned} \Delta f_{d\max} &\approx \frac{f_o e}{c} (10,087.5) (1) (0.1503) (2\sqrt{2}) \\ &= \frac{f_o e}{c} 4.30 \times 10^3 = \frac{e}{\lambda_f} 4.30 \times 10^3 \quad [\text{cps}] \quad (2-8) \end{aligned}$$

where λ_f is the transmitted wavelength in feet. Thus for $f_o = 6 \text{ kmc}$, $\lambda_f = 0.1637 \text{ foot}$, $e \approx i = 0.00175$ (0.1 degree)

$$\Delta f_{d\max} \approx \frac{(1.75)(4.30)}{0.1637} = 46 \text{ cps} \quad (2-9)$$

From the brief discussion above it is seen that the voice quality and crosstalk, associated with a doppler-shifted single-sideband voice channel, can be related with the cyclical station-keeping tolerances identified by the orbital parameters i, e , and θ .

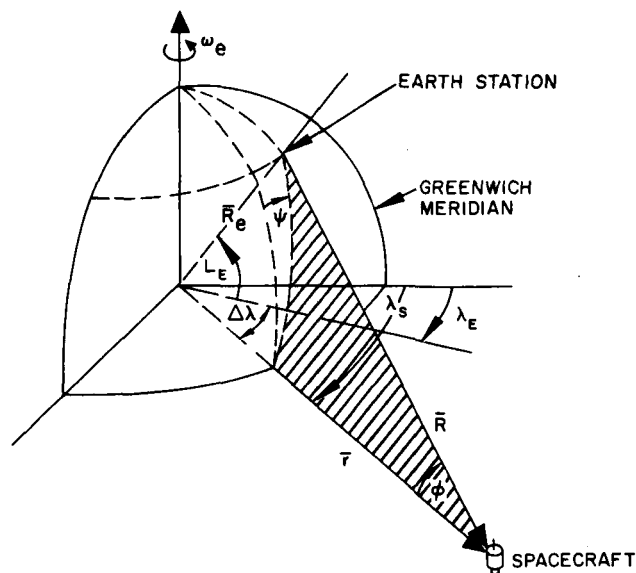


Figure 2-1. Spacecraft-Earth Station Geometry

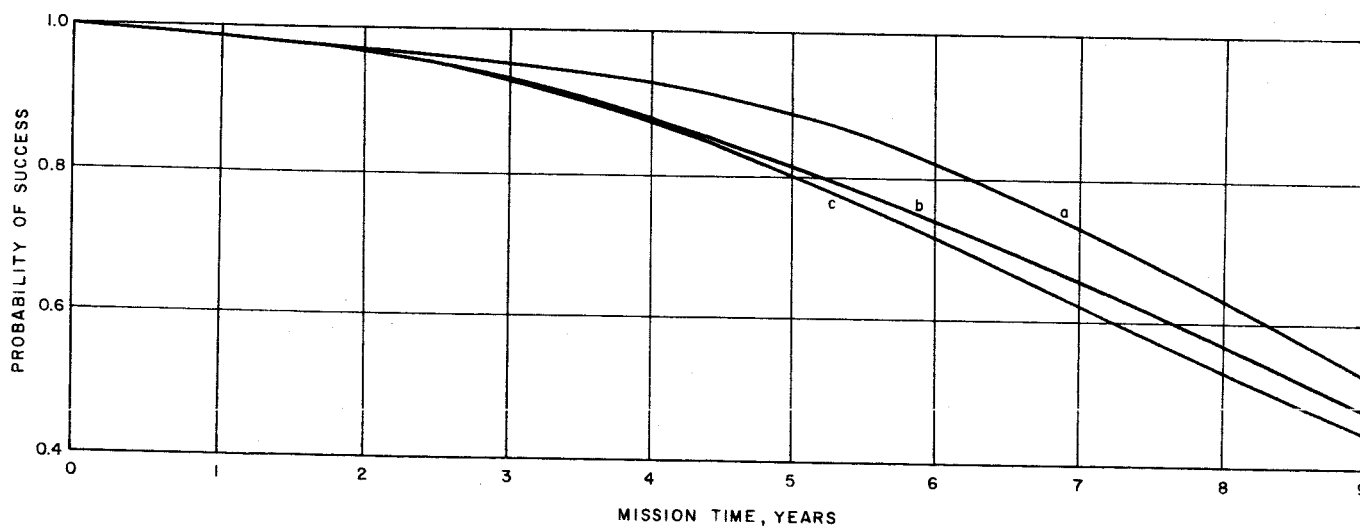
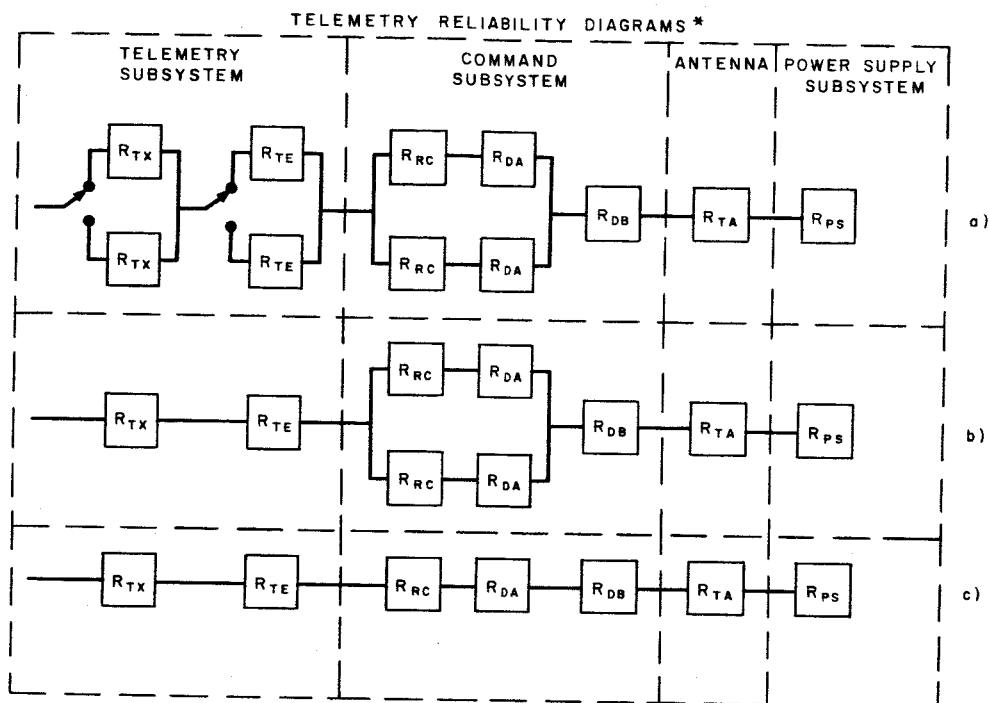
SYSTEM RELIABILITY STUDIES

Design Analyses

The telemetry and command subsystem reliability models presented in the Initial Project Development Plan (15 August 1962 - Figure 6-69), have been examined to determine the amount of degradation in telemetry mission success when a nonredundant configuration is employed in each spacecraft quadrant.

The results are shown in Figure 2-2. Curves a, b, and c show the predicted probabilities of telemetry mission success as a function of time for configurations a, b, and c respectively. These predictions indicate that inter-quadrant redundancy is adequate and that the removal of one telemetry transmitter and encoder and one command receiver and decoder in each quadrant will not substantially degrade the telemetry mission reliability during the 3- to 5-year spacecraft mission time.

Since the command subsystem is also required for the multiple access and frequency translation communication modes of operation, the effect of the nonredundant quadrant command configuration upon communications mission success has been evaluated. An analytical comparison of the communication reliability exhibited with the simplified configuration yields no significant variation in the curves presented in the September Monthly Progress Report, Figures 2-3 and 2-4.



* ONLY ONE QUADRANT OF THE TELEMETRY AND COMMAND SUBSYSTEMS IS SHOWN

Figure 2-2. Probability of Telemetry Mission Success

Therefore, the nonredundant configuration represented by Figure 2-2, diagram c, has been recommended to be incorporated as the Syncom II spacecraft design. This configuration will yield a high probability of obtaining telemetry data during the lifetime of the spacecraft; it will not result in a degradation in the communications mission; it will simplify interconnections and switching, enhancing reliability; and it will result in an overall reduction in weight of the spacecraft.

The curves presented in Figure 2-2 include the effect of the telemetry subsystem, command subsystem, power supply subsystem, and antenna which are each required for successful completion of the telemetry mission. The analyses and recommendations presented assume that any quadrant of the telemetry subsystem will sample and transmit the required spacecraft data. Thus, the quadrants are assumed to operate sequentially with one required to survive for mission success. (Previous analyses of the telemetry subsystem have been based upon a binomial operation.)

As before, it is assumed that all command receivers must be energized, but that the decoders have a low duty cycle and that one quadrant of the command subsystem will provide the necessary spacecraft commands.

The analyses and recommendations presented are further based upon a minimum number of encoder and decoder channels, 64 and 55, respectively. Although the spacecraft may require more channels resulting in a degradation of the estimates discussed, the percent relative deviation among the curves representing each configuration should not change. The tradeoffs among redundancy, reliability, cost, and weight will be further examined if a substantial increase in the encoder and decoder complexities results upon definition of the spacecraft design.

COMPONENTS AND MATERIALS

During the report period applicable Syncom I drawings and a preliminary bill of materials were reviewed for planned Syncom II use. Some parts will require new specifications. For others, preferred alternatives are being recommended to the circuit engineers for incorporation in their designs.

A basic addendum document, modifying the existing procurement specifications for transistors, was prepared and is being revised for applicability to other types of devices. This addendum adds requirements expected to aid in securing parts of high reliability.

Some of the frequency-control crystals used in the engineering model electronics were reported by the manufacturer to have a possible spurious mode of operation, which, however, is not considered detrimental for their proposed use. Additional crystals have been secured for confirmation testing, which is now in process.

It had been considered that certain tantalum capacitors used on Syncom I and contemplated for Syncom II might fail as a result of excessive charging current rates, but tests failed to confirm this. No failures resulted from tests employing the maximum feasible charging rates. The possibility of reverse-current surges is now being investigated.

Tests of ultraviolet exposure of three thermal control paints continued during the period. One of the paints is an inorganic type, which may have greater stability than the other two. These tests are being made as a first specific part of the study program to extrapolate short-term observations to predict the potential long-term life of a number of materials and parts.

A high-temperature encapsulating compound for the traveling-wave tube is being investigated in vacuum.

3. ADVANCED TECHNOLOGICAL DEVELOPMENT

DUAL-MODE TRANSPONDER

Laboratory Integration of Transponders

Both the frequency translation and multiple-access transponders were installed in the spacecraft and operated satisfactorily during the predemonstration checkout period. No major problems were encountered during the integration.

Quantitative noise power ratio and intermodulation distortion measurements were not taken during the report period due to existence of an undesirably high noise level in the test transmitter of the simulated ground station.

Circuits Common to Frequency Translation and Multiple-Access Transponders

Input Mixers (6 kmc) (Figure 3-1)

Assembly and fabrication of the required single mixers is now complete. Effort has been initiated to improve the critical adjustment of the T-junction and associated transmission line to each mixer. Design for the improvement of local oscillator isolation to the IF terminal is also being conducted.

Hybrid (4 kmc)

The units required were completed and placed in operation in the demonstration model.

X32 Multiplier and Bias

Completed units were employed in the spacecraft and an additional unit has been integrated into the ground checkout equipment.

A concerted effort has been initiated to improve the stability of the X32 frequency multiplier chain. This will include increasing the range of

temperature, voltage, and load mismatch, over which stable operation can be achieved. These improvements should also allow the multipliers to be more readily reproducible.

X2 Multiplier (Figure 3-2)

The units required for the spacecraft transponders and ground equipment are now in service. An effort has been initiated to improve the efficiency prior to finalizing production design.

Circuits for FM Frequency Translation Transponder

25-mc Preamplifier/25-mc IF Amplifier

As stated in the last report, these two units were combined. However, further investigation showed that their operation as separate units would provide an improved gain distribution and packaging design.

25-mc Limiter

The remaining unit is still undergoing final checkout.

High-Level and Beacon Mixers

An effort is being made to reduce the RF "leakage" from the IF terminals. Units are now in service in the spacecraft and in the ground equipment.

Hybrids for the high-level mixer were fabricated and placed in service for the demonstration. They were integrated with the diodes to complete the combined high-level and beacon mixer configurations.

Master Oscillator (66 mc)

These units are now in service in the spacecraft and ground equipment. Additional units will be used for further testing.

Circuits for Multiple-Access Transponder

IF Phase Modulator

Units have been modified, checked out, and now satisfactorily meet the design sensitivity requirements.

5.5-mc Bandwidth Preamplifier

The remaining unit has been modified to meet requirements and is now complete.

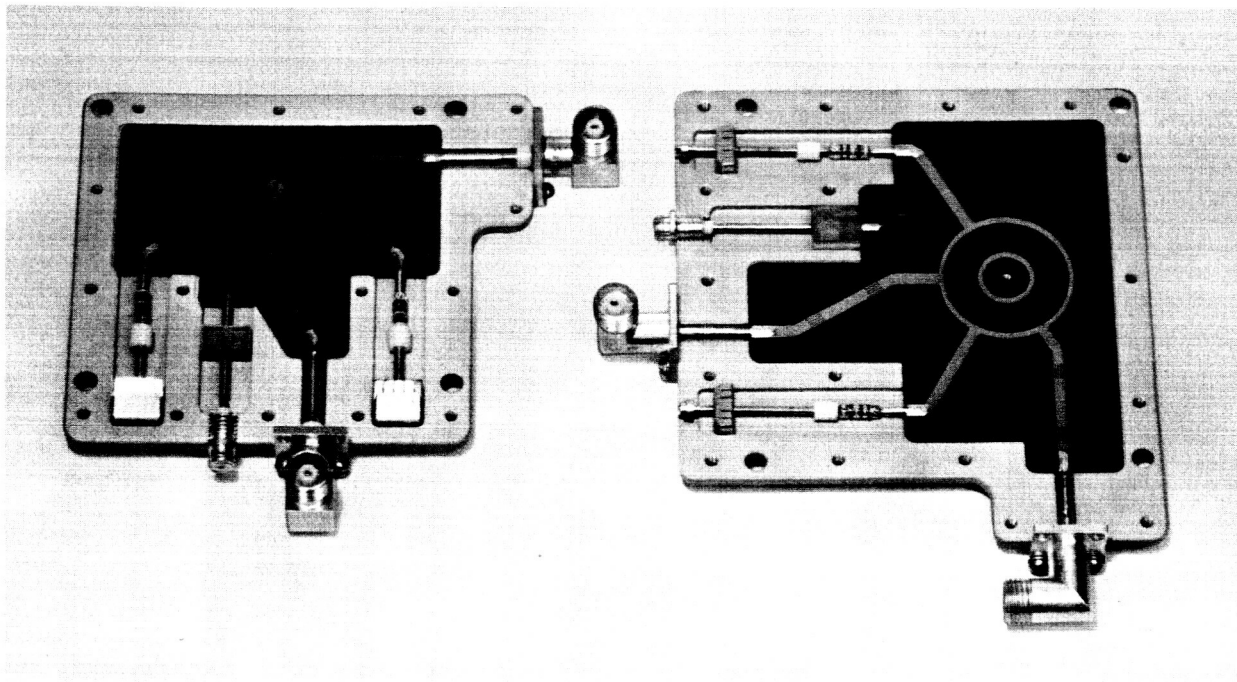


Figure 3-1. Comparison of Syncom I (left) and Syncom II (right Input Mixers

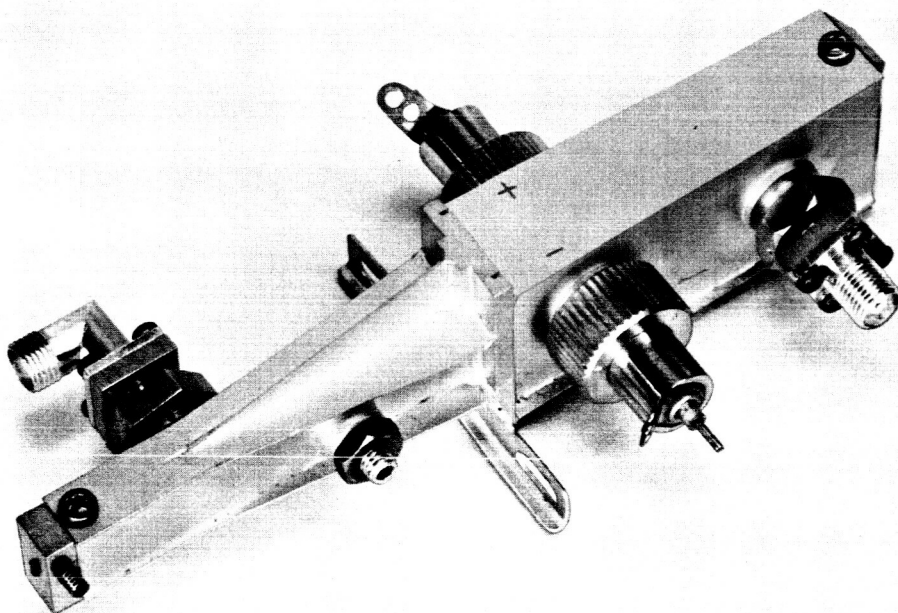


Figure 3-2. X2 Multiplier

Receiver Master Oscillator (66.223 mc)

The remaining units were checked out and met all design requirements.

Transmitter Master Oscillator (32.5mc)

Completion of these units was accomplished during the report period.

TRANSPONDER TEST AND DEMONSTRATION PANEL

This equipment (Figure 3-3) was completed during the report period. It was used in the predemonstration checkout of the engineering model of Syncom II communications transponders.

A traveling-wave tube amplifier was added to the transmitter unit to bring the output up to the 20-milliwatt level.

The R-C filter in the AFC unit was modified in order to achieve stable phase lock of the pilot signal.

The equipment successfully demonstrates the multiple-access transponder by sending and receiving voice signals in the presence of 55 other test signals. Speech quality was good with low background noise.

The frequency translation transponder was demonstrated by sending television pictures through the satellite. Picture quality of the relayed picture was approximately identical to the transmitted picture.

Quantative noise power ratio measurements of the Syncom II transponder were not taken at this time. Measurement of noise was not possible due to noise in the test transmitter of the simulated ground station. Changes are being incorporated to reduce residual noise in the test transmitter to preclude masking noise in the transponder. The noise power ratio tests will evaluate both noise created by intermodulation distortion and residual system noise. Also, direct linearity measurements on the test transmitter will be made.

TRAVELING-WAVE TUBE (Figure 3-4)

The qualification model traveling-wave tube (384H-8) developed an air leak in the vacuum seal after it was shipped and awaiting test. The fault was traced to a faulty vacuum pinchoff. This resulted in a slow leak in the vacuum envelope.

In prepackaged testing, two tubes (384H-13 and 384H-17) met the performance requirements. Except for a 10 percent increase in helix pitch, these tubes are identical in construction to No. 384H-8.

Although the above design meets performance requirements, optimum operation is near the low end of the specified frequency band. To correct

this condition, a tube having a 10 percent reduction in helix diameter and a 15 percent decrease in helix pitch is being constructed. This tube will be tested during the next period.

PHASED ARRAY TRANSMITTING ANTENNA

The phased array was coupled to the engineering model control electronics and, following minor wiring modifications, operated satisfactorily.

Array Development

A new version of the vertically polarized antenna was fabricated, using larger diameter tubing and center conductor in the coaxitube configuration. This eases the tolerances and assembly problems. The antenna consists of four slot-fed half-wave dipoles mounted collinearly. The initial attempt at matching the antenna resulted in a VSWR of less than 1.5 over a 200-mc band centered at 4100 mc. However, the addition of the fiberglass sleeves did change the result slightly, indicating that minor changes have to be made in the matching sections.

RF Circuits

The design of the all-stripline output coupler is nearing completion. This includes the vertical stripline-to-stripline transition, the vertical TM-to-stripline coupler, and a new 90-degree square hybrid, in which the input and output arms are connected at 45-degree angles to the square (Figure 3-5). The exact layout required a number of attempts due to requirements of symmetry, isolation between adjacent striplines, and equal phase lengths from input probes to output TM connectors.

Control Electronics

Engineering Model Control Electronics

The change described in the Advanced Syncom January report, which eased the requirements of the ψ signal frequency stability and simplified beam direction correction, was completed during this reporting period. The updated control electronics were then checked out. The entire phased array transmitting antenna was integrated and checked out, using a simulated transponder.

The control electronics were then integrated and checked out in the spacecraft. All features of the control electronics were tested with the spacecraft spinning. The entire communication subsystem was then integrated into the spacecraft and the subsystem was checked out with the spacecraft spinning.

Spacecraft Electronics - Jet Control Electronics

Figure 3-6 is a block diagram of the phased array and pulse jet control electronics.

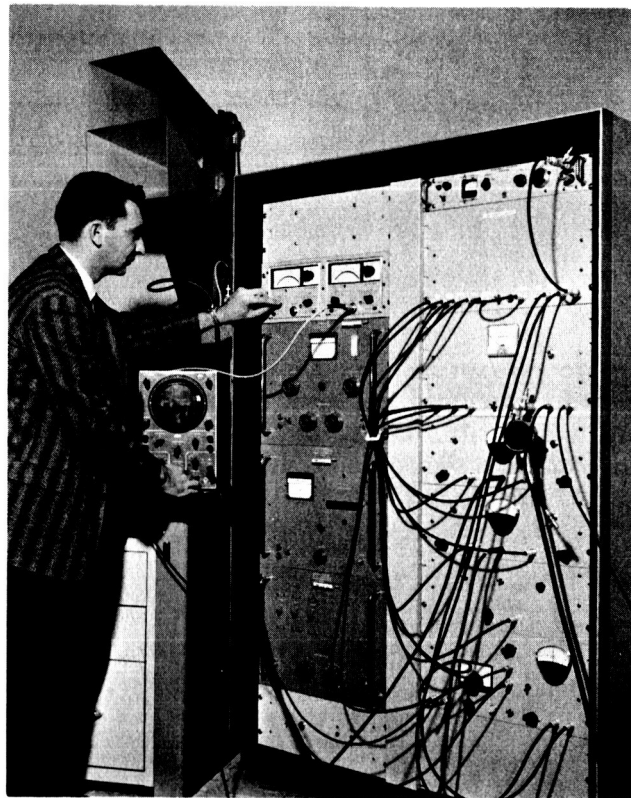


Figure 3-3. Transponder Test and Demonstration Panel

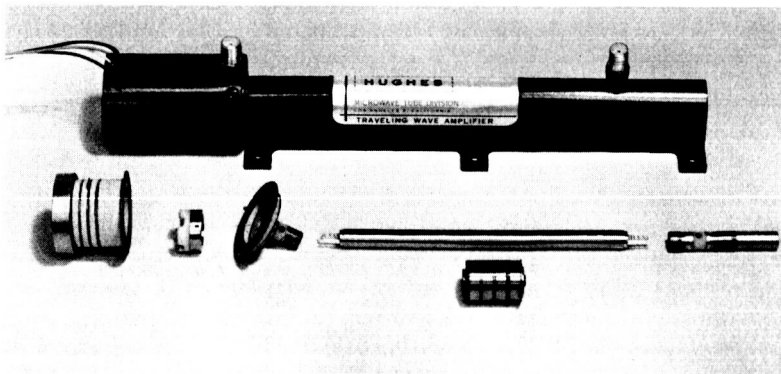


Figure 3-4. 4-Watt (384-H)
Traveling-Wave Tube

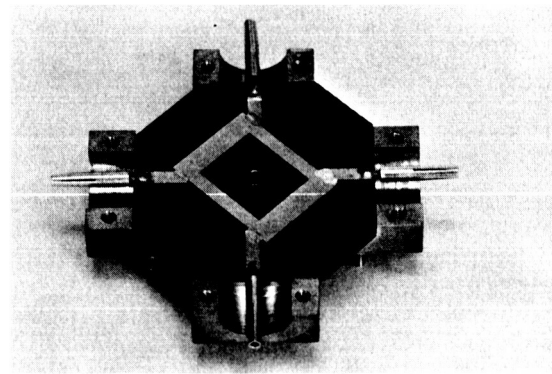


Figure 3-5. 4-kmc, 3-db
Hybrid Coupler

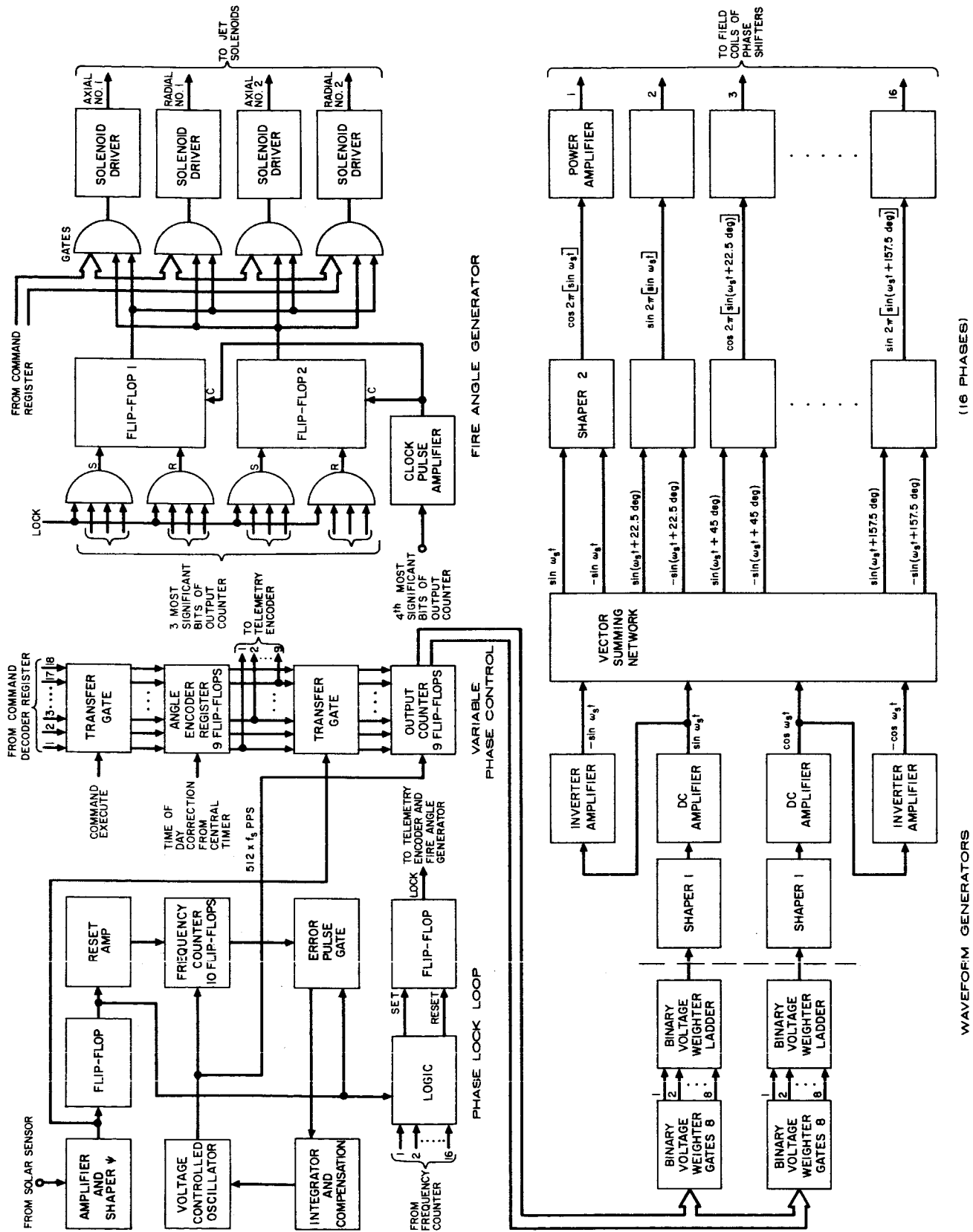


Figure 3-6. Syncrom II Phased Array and Pulse Jet Control Electronics

The fire angle generator has been simplified. It now has 74 percent or 229 fewer components in the solenoid driver control electronics. When the antenna beam is directed at the earth, the output counter has a count of zero when the zero antenna element is on the spacecraft-earth line. If the relative position of the zero antenna element to the four jets is known (it must be some multiple of 22.5 degrees), then the gating to FF1 and FF2 (Figure 3-6) can be earth referenced. Figure 3-7 shows how FF1 and FF2 will be used. FF1 is set when J1 reaches 67.5 degrees.

The outputs of the two flip-flops are then gated with the command decoder register so that J1 and J2 can both be fired in the 90-degree sector in the same cycle. To correct roll the axial jets should be fired at +90 or -90 degrees. However, the two axial jets (J3 and J4) are ± 90 degrees with respect to the two radial jets (J1 and J2). By commanding the antenna beam 90 degrees away from the spacecraft-earth line, FF1 and FF2 are now a correct timing reference for roll correction by the two axial jets.

The gates (which control the solenoid drivers) select through the command register those jets that are to be fired in which sectors.

Waveform Generators and Amplifiers

The waveform generators and amplifiers have been modified to achieve simplicity of design, reduction of part count, and reduction of power dissipation. The new circuit configurations are shown in Figures 3-8, 3-9, and 3-10. These configurations result in a parts count savings of approximately 34 percent and reduce power dissipation by 50 percent.

The adding network, Figure 3-8, is identical to the previous adder with the exception that eight more circuits are added. These additions are necessary to obtain the complements of the waveforms obtained by the previous eight waveform adders. The inputs to the adder network are:

$$e_a = A \sin 2 \pi f t$$

$$e_b = A \cos 2 \pi f t$$

$$e_c = -A \sin 2 \pi f t$$

$$e_d = -A \cos 2 \pi f t$$

The 16 outputs are of the form

$$e_{an} = \frac{A}{\sqrt{2}} \sin \left(2 \pi f t + \frac{n\pi}{8} \right) \quad n = 0, 1, 2, \dots, 15$$

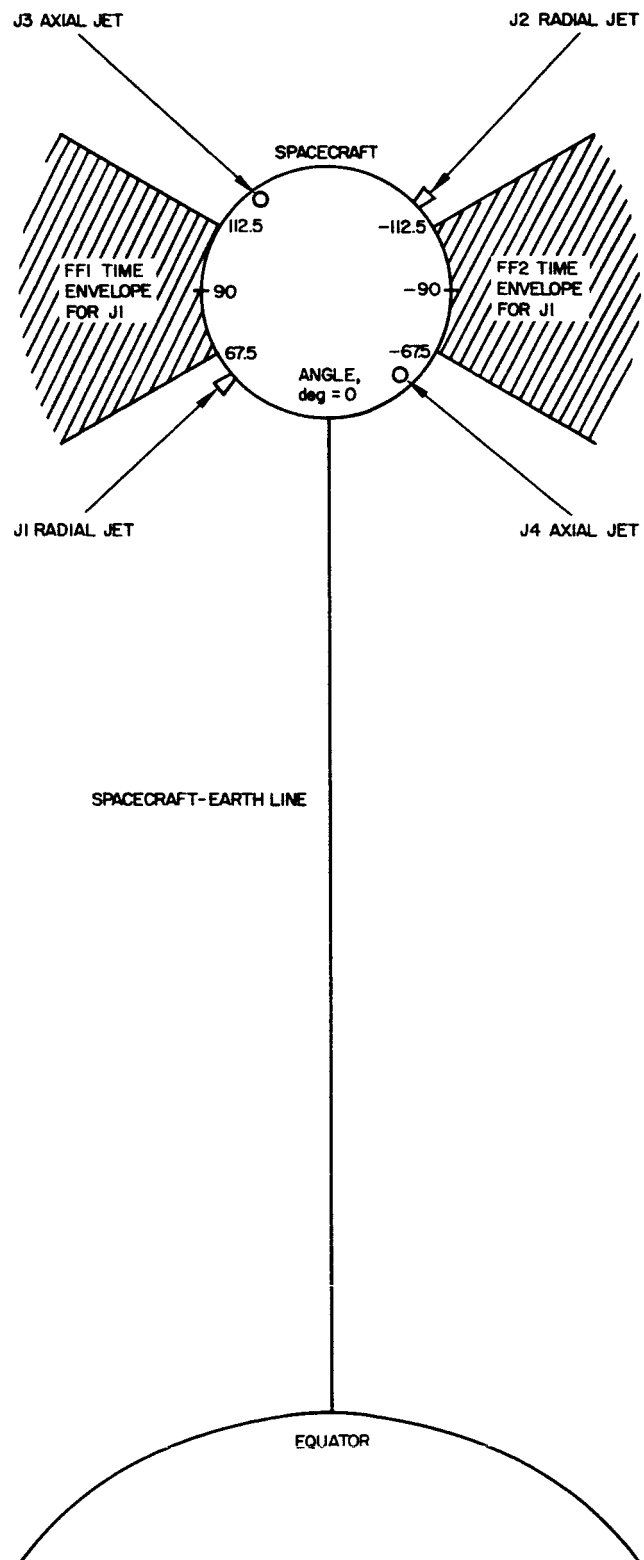
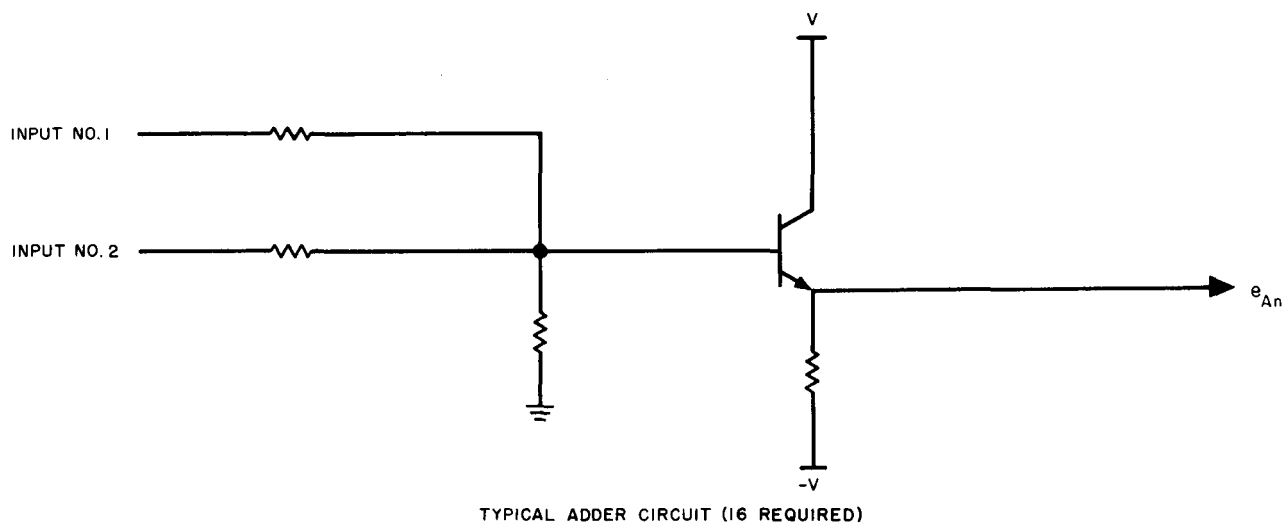


Figure 3-7. Syncom II Jet Control



TYPICAL ADDER CIRCUIT (16 REQUIRED)

INPUT NO. 1	INPUT NO. 2	OUTPUTS
$A \sin 2\pi ft$	$A \cos 2\pi ft$	$e_{An} = \frac{A}{\sqrt{2}} \sin \left(2\pi ft + \frac{n\pi}{8} \right) \quad n = 0, 1, 2, 3$
$A \cos 2\pi ft$	$-A \sin 2\pi ft$	$e_{An} = \frac{A}{\sqrt{2}} \sin \left(2\pi ft + \frac{n\pi}{8} \right) \quad n = 4, 5, 6, 7$
$-A \sin 2\pi ft$	$-A \cos 2\pi ft$	$e_{An} = \frac{A}{\sqrt{2}} \sin \left(2\pi ft + \frac{n\pi}{8} \right) \quad n = 8, 9, 10, 11$
$-A \cos 2\pi ft$	$A \sin 2\pi ft$	$e_{An} = \frac{A}{\sqrt{2}} \sin \left(2\pi ft + \frac{n\pi}{8} \right) \quad n = 12, 13, 14, 15$

Figure 3-8. Adder Network

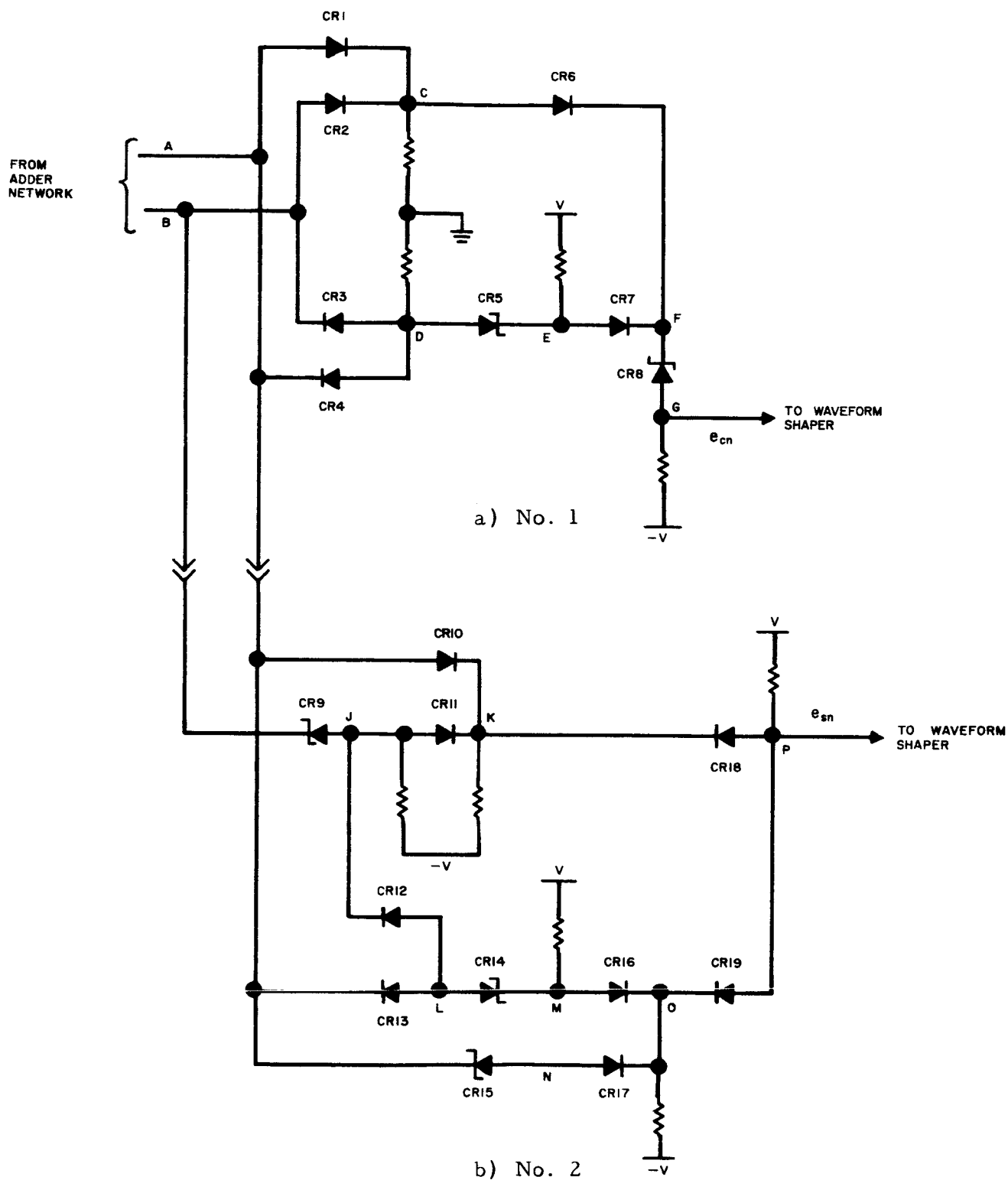


Figure 3-9. Waveform Generators No. 1 and 2

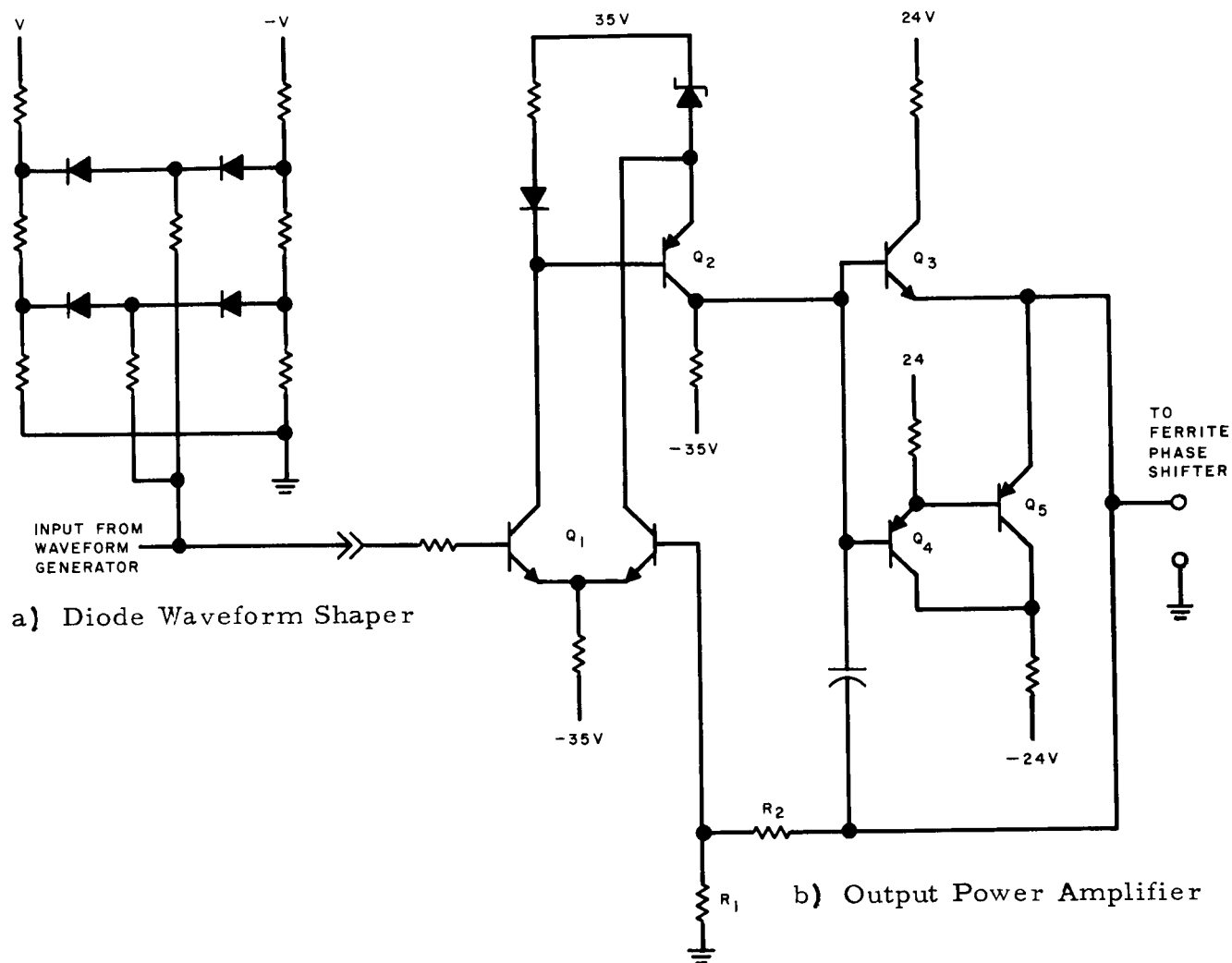


Figure 3-10. Waveform Shaper Amplifier

The ferrite phase shifters require 16 signals of the form:

$$\left. \begin{aligned} e_{cm} &= B \cos 2\pi \left(\sin \left(2\pi ft + \frac{m\pi}{8} \right) \right) \\ e_{sm} &= B \sin 2\pi \left(\sin \left(2\pi ft \pm \frac{m\pi}{8} \right) \right) \end{aligned} \right\} m = 0, 1, 2, \dots, 7$$

where the zero-to-peak magnitude, B , is 20 volts.

To obtain the desired ferrite phase shifter signals, three operations are performed on the adder network output signals. These operations are shown schematically in Figure 3-11.

Waveform generator 1, Figure 3-9a, produces a close approximation to the e_{cm} signals, and waveform generator 2, Figure 3-9b, produces a close approximation to the e_{sm} signals.

Both waveform generators are implemented with the use of a combination of "greater" and "lesser" gates. Also, zener diodes are used to shift the signal's dc bias where necessary as the signal passes through the circuit.

The inputs to waveform generator 1 are e_{an} and $e_{a(n+8)}$, where e_{an} is a signal phase shifted $n\pi/8$ radians from the reference and $e_{a(n+8)}$ is the complement of e_{an} . Diodes CR1 and CR2 form a "greater" gate. Thus, the signal at point C will be a positive full-wave rectified sinusoid, since the gate passes the positive half cycle of e_{an} and then the positive half cycle of $e_{a(n+8)}$. The gate output is shown in Figure 3-12. The waveforms at nodes noted by a capital letter are also shown in Figure 3-12. Diodes CR3 and CR4 form a "lesser" gate, thus producing at its output, point D, a negative full-wave rectified signal.

The zener diode CR5 shifts the bias of signal D positively $A/2$ volts. The result is signal E.

Diodes CR6 and CR7 form another "greater" gate whose output is signal F. Signal F is then bias shifted negatively to produce an output signal which is symmetrical about ground.

The output of waveform generator 1 is, to a rough approximation, the cosine of the input signal or:

$$\text{Waveform generator 1 output} \cong R \cos 2\pi \left[K \sin \left(\omega t + \frac{m\pi}{8} \right) \right].$$

To better approximate the desired signal, the waveform generator output is passed through a diode waveform shaper, Figure 3-13a, which smoothes the

positive and negative peaks such that the input to the power amplifier is as shown in the figure.

To obtain the e_{sm} signal which is in phase with the e_{cm} signal just described, the same inputs are applied to waveform generator 2, as shown in Figure 3-9b.

Zener diode CR9 shifts the bias of $e_{a(n+8)}$ negatively, as shown by J, in order to obtain a rectified waveform with unequal conduction. The positive rectified waveform is K and is produced by the "greater" gate composed of diodes CR10 and CR11. Applying the waveforms of A and J to the "lesser" gate, composed of CR12 and CR13, and then shifting the bias yields the waveform M. By shifting the bias of e_{an} and applying the result, N, along with M into a "greater" gate, CR16 and CR17, the waveform O is produced. The remaining operation necessitates applying waveforms O and J to the "lesser" gate, formed by CR18 and CR19, to obtain the waveform P, which is an approximation to the sine of the input or

$$\text{Waveform generator 2 output} \cong \sin 2\pi \left[\sin \left(2\pi ft + \frac{m\pi}{8} \right) \right].$$

As with the previous waveform, it remains to smooth the positive and negative peaks to obtain a better approximation. A diode waveform shaper, identical to the previous one, accomplishes this operation with the result that the power amplifier input will be as shown in Figure 3-13b.

Output Power Amplifier. This amplifier is a high-gain dc amplifier employing resistive feedback for stable operation and complementary emitter followers in the output stages for low output impedance. Transistors Q1 are a closely matched pair, packaged in one standard T0-5 transistor case, operating as a differential amplifier. Since the circuit open-loop gain is much larger than unity, the closed-loop voltage gain is very nearly $(R1 + R2)/R1$ with no phase reversal. Transistor Q4 is incorporated to reduce the power dissipation of the circuit.

COLLINEAR ARRAY RECEIVING ANTENNAS

Vertical Polarization

During this report period optimization of the flared length of the dipole was investigated. A series of radiation pattern characteristics were taken, yielding the data in Table 3-1.

Figure 3-14 shows the antenna assembled and "exploded." Since using a uniform distribution (with four elements) which produces a beam that is too narrow, a tapered distribution will be used. Coupling coefficient of the elements will be adjusted by varying the thickness of the dielectric spacers.

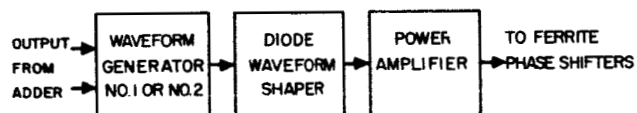


Figure 3-11. Operations on Day Shifter Excitation Signals

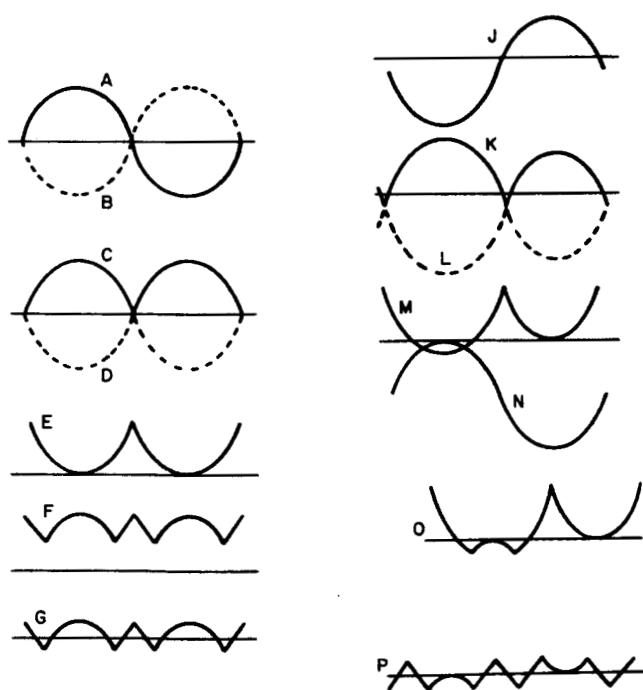


Figure 3-12. Waveforms of Generator Nos. 1 and 2

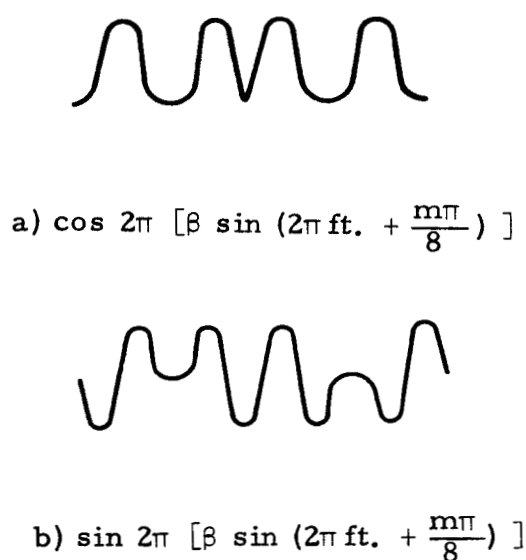
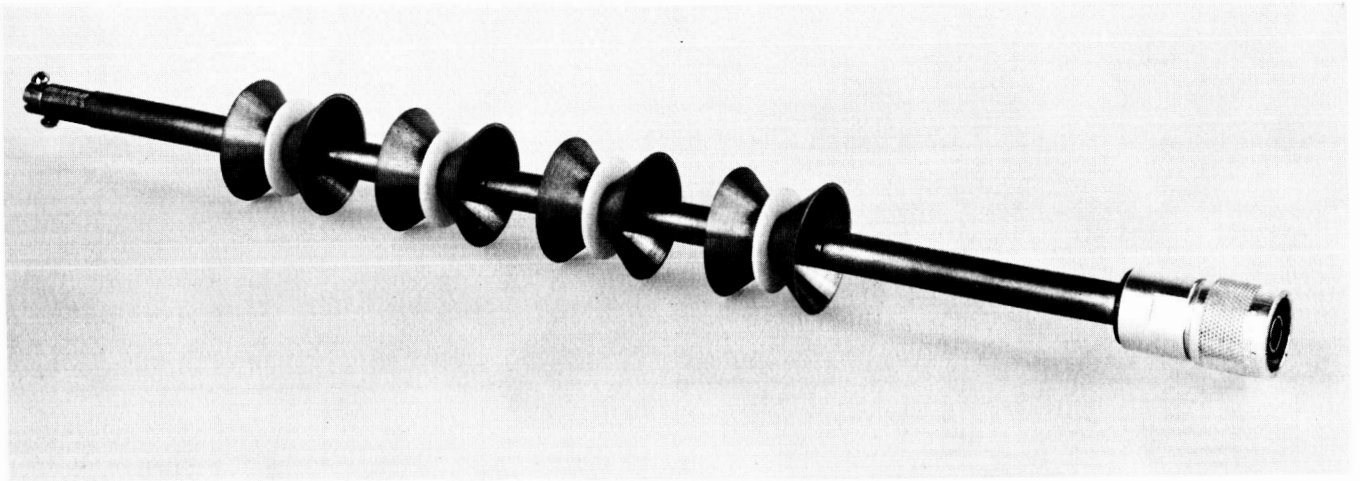
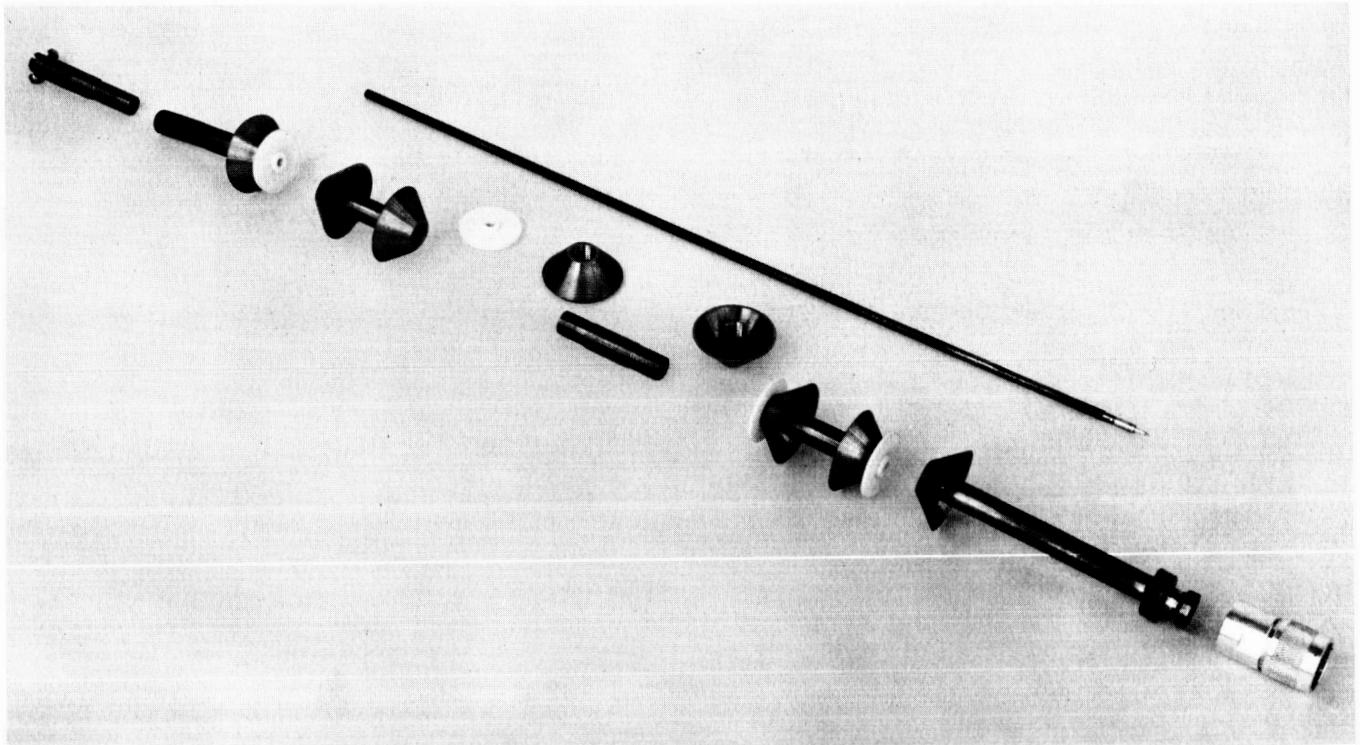


Figure 3-13. Waveform Generator Outputs



a) Assembled Prototype



b) Exploded Prototype

Figure 3-14. Syncom II Flared Dipole Antenna

TABLE 3-1. RADIATION PATTERN CHARACTERISTICS

Design frequency: 6300 mc
 Desired bandwidth: 200 mc
 E-plane radiation pattern - Vertical polarization
 Diameter: $0.500 \lambda_0$

Parameter	Frequency, mc							
	5800	5900	6000	6100	6200	6300	6400	6500
High-power bandwidth, degrees	17.50	16.50	14.50	13.50	13.00	12.50	13.00	12.50
First sidelobe level, decibels	-11.75	-9.25	9.75	9.25	-10.25	-10.00	-11.50	-11.00
Flare Length:	$0.500 \lambda_0$							
High-power bandwidth, degrees	18.50	15.50	14.00	13.00	13.50	13.50	13.00	12.00
First sidelobe level, decibels	-14.50	-11.75	-11.00	-10.75	-10.00	-10.00	-7.50	-4.00
Flare Length:	$0.400 \lambda_0$							
High-power bandwidth, degrees	17.50	15.50	14.00	12.50	12.50	12.50	12.50	12.00
First sidelobe level, decibels	-15.50	-12.00	-11.75	-12.00	-11.50	-11.50	-12.00	-11.50
Flare Length:	$0.300 \lambda_0$							

Analyzing the data, it is seen that no appreciable change is noticeable in the overall radiation pattern characteristics. The data show that the beam-width of the antenna is nearly constant within ± 0.25 degree over a frequency range of 400 mc centered at 6300 mc.

No attempt has been made to optimize the input matching characteristics. The knowledge acquired on the scaled-up version of the Mark I antenna is expected to expedite this effort.

During this report period, the interim receiving antenna, which consists of a scaled-up version of the Mark I receiving system, was completed.

Horizontal Polarization

Cloverleaf Arrays

A second six-element cloverleaf array has been fabricated for operation at 3830 mc (Figure 3-15). The impedance of this array is almost identical to the first array fabricated. The two 3830-mc cloverleaf arrays were used in a mutual coupling measurement. This measurement was made under two conditions: 1) with the cloverleaf sections adjacent, and 2) with the cloverleaf sections staggered. (See Figure 3-16.) The results of the mutual impedance measurements are shown in Figures 3-17 and 3-18. The characteristic impedance of the coaxial line of the array is 50 ohms.

A scaled model of the 3830-mc six-element cloverleaf array has been fabricated (Figure 3-15). This scaled model was designed to operate at 6300 mc. Impedance measurements indicate that this array is resonant at approximately 6320 mc. The VSWR of the array as a function of frequency for the 200-mc bandwidth is shown in Figure 3-19. The VSWR at 6300 mc is 1.23:1, which is suitable for system tests; therefore, this array will be used for system tests without any additional impedance matching. E-plane and H-plane antenna patterns have been made across the 200-mc frequency band.

The typical patterns are shown in Figure 3-20. The major characteristics of this array are tabulated below:

<u>Frequency, mc</u>	<u>Omnidirectionality, db</u>	<u>Beamwidth, degrees</u>	<u>Sidelobe Level, db</u>
6200	0.75	19.1	11.2
6225	0.65	19.2	12.3
6250	0.75	19.3	12.1
6275	0.75	18.9	12.0
6300	0.70	18.4	11.7
6325	0.65	18.4	11.5
6350	0.70	18.1	11.4
6375	0.65	18.9	11.7
6400	0.50	19.0	11.8

The antenna gain measurement will be accomplished during the next report period.

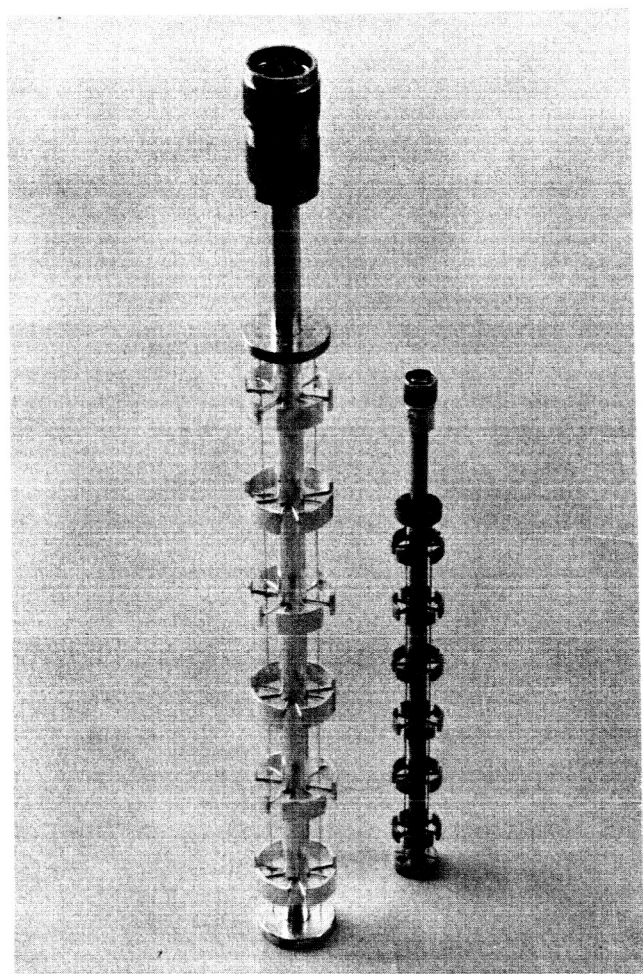


Figure 3-15. Syncom II Cloverleaf Arrays
for 4 kmc Band (left) and 6 kmc
Band (right)

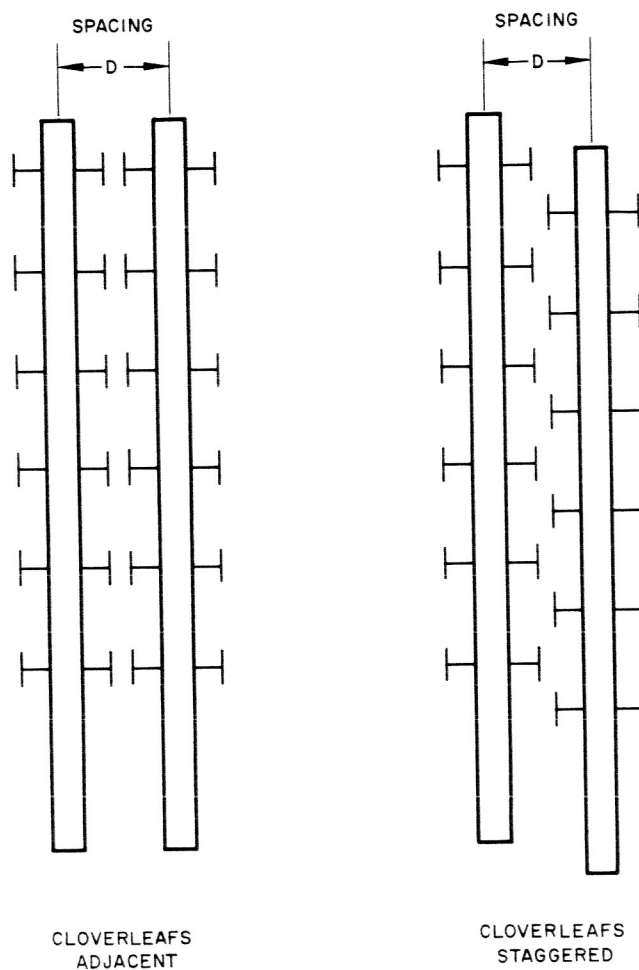


Figure 3-16. Mutual Coupling
Measurement Configuration

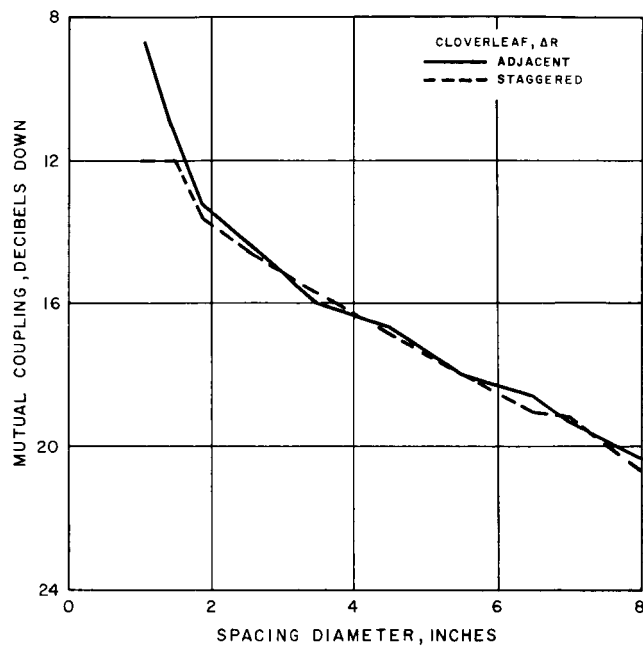


Figure 3-17. Mutual Impedance Measurements

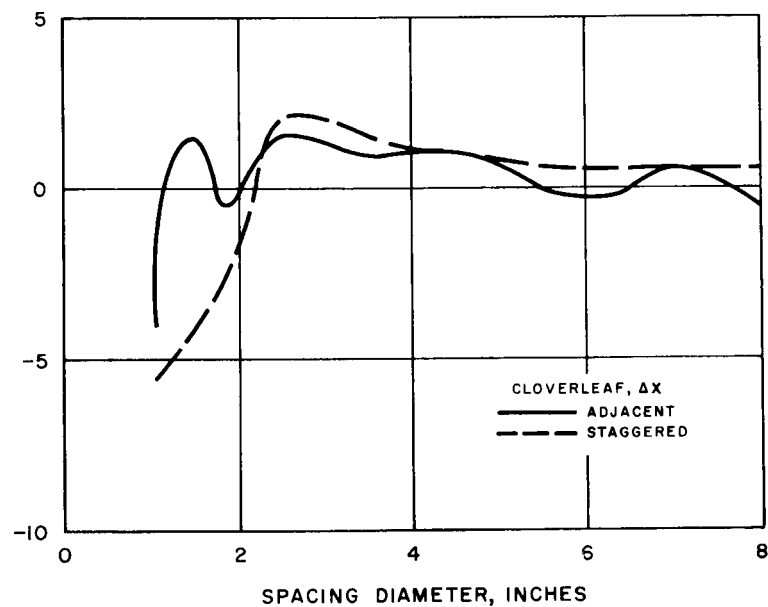
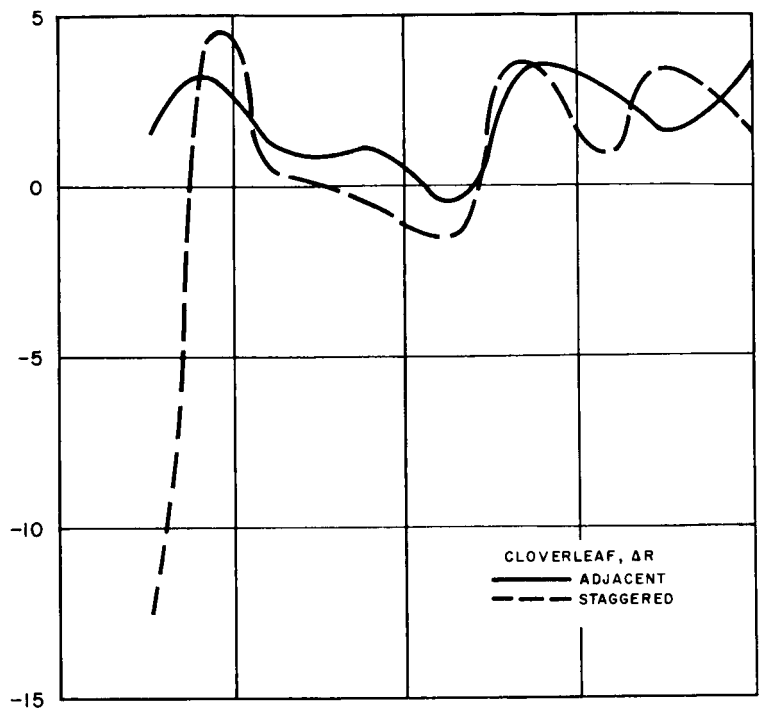


Figure 3-18. Mutual Impedance Measurements

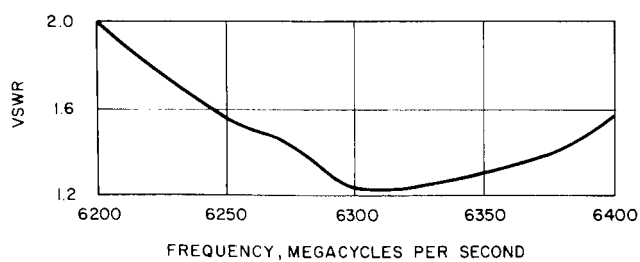


Figure 3-19. VSWR, 6300 mc Cloverleaf Array

Broadside-Firing Helix

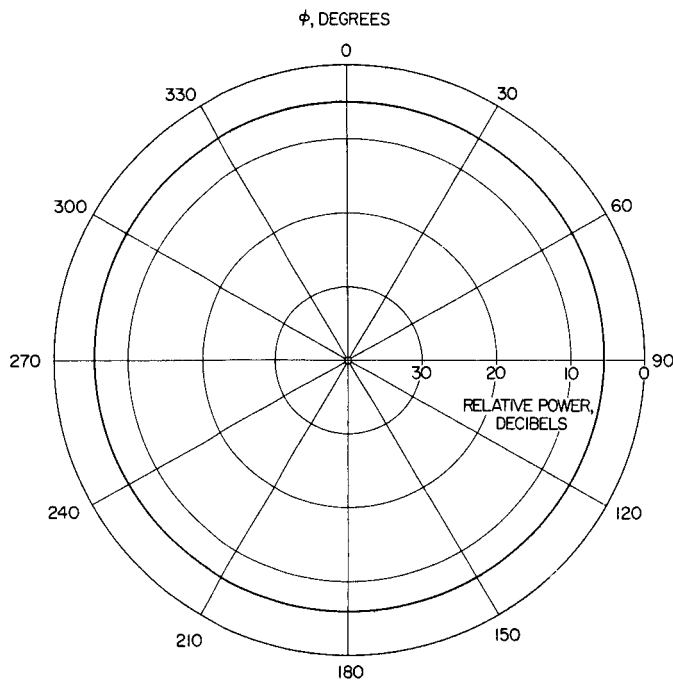
A broadside-firing helix antenna (Figure 3-21) consisting of two equal, oppositely wound, collinear wire helices supported on a coaxial metal mast was designed and fabricated. The radiation is polarized principally in a plane perpendicular to the axis; the small cross-polarized component is made to cancel by winding the helices in opposite senses. If the pitch and diameter are adjusted so that the length of a helical turn is an integral number of wavelengths, and each turn is separated by a half-wavelength (p), the radiation pattern in the plane perpendicular to the axis (azimuth) is independent of azimuth angle and the pattern in the elevation plane has the directivity normally associated with a linear array of cophased sources. A theoretical analysis reveals that care must be taken to get a traveling wave of current on the helix to obtain an omnidirectional azimuth pattern. This latter condition may be effected by adjusting helix-to-mast spacing which has the effect of varying the radiation per turn. This configuration has good broad-band characteristics, such as those expected from helical antennas in general. The linear dimensions are proportional to wavelength, so that the antenna is easily scaled with frequency.

An initial model of such an antenna for operation at 4 kmc has been constructed and preliminary data obtained. The azimuthal pattern is shown in Figure 3-22. The omnidirectionality is ± 1.75 db, and the half-power beamwidth in elevation is 8 degrees. Because of standing waves of current on the helices, it was necessary to terminate them with resistors to achieve the pattern shown in Figure 3-22. The antenna is now being modified so that the helix-to-mast spacing will be increased. This will increase the radiation per turn and thereby reduce the reflected wave. This will also reduce the effective length of the antenna, resulting in increased beamwidth in the elevation plane.

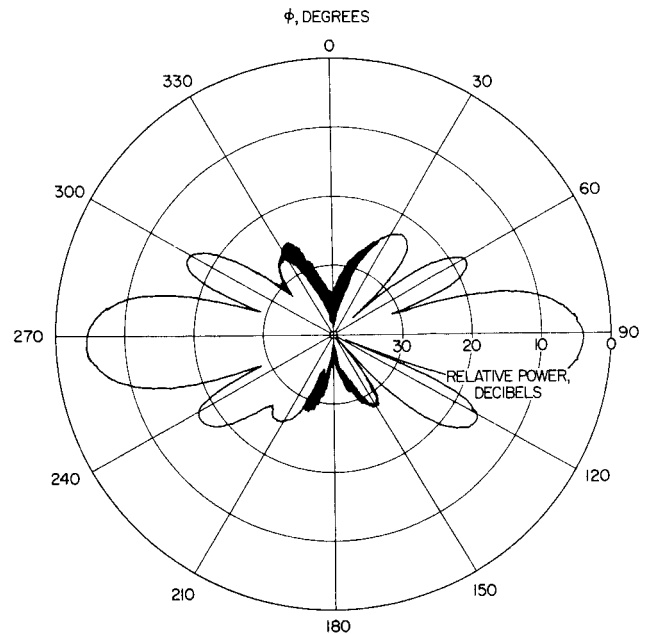
Coaxial Slot Array

This design effort has been conducted as a backup effort for the element arrays of the phased array. The objective has been to develop a coaxial antenna element with an array of slots which will meet the following requirements:

- 1) The E-plane pattern is to be perpendicular to the element axis and be omnidirectional within ± 1 db.
- 2) The H-plane pattern is to contain the element axis and have a mainlobe beamwidth of 17.3 degrees minimum.
- 3) The element gain is to be at least 7 db above isotropic.
- 4) The sidelobes shall be nominally 13 db below the main beam.
- 5) The impedance match of the element is to be such that the maximum VSWR will not exceed 1.5:1 over the 200-mc bandwidth of the phased array.



a) E-Plane



b) H-Plane

Figure 3-20. Cloverleaf Array Antenna Pattern

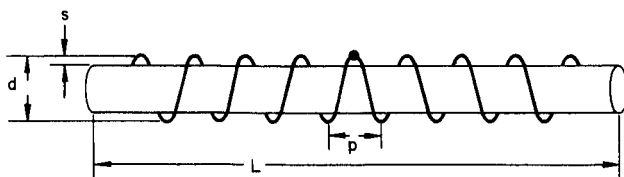


Figure 3-21. Broadside Firing Helix

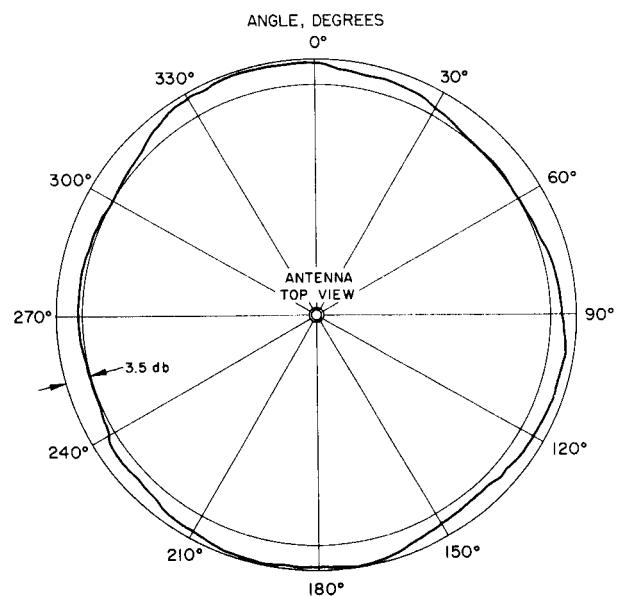


Figure 3-22. Azimuth Pattern, 4 kmc Broadside Firing Helical Antenna

In general, the approach under development is to use slots parallel to the element axis. These slots in the outer conductor are excited by a unique design of a helical ridged center conductor.

A number of configurations have been constructed and tested. The most promising model to date is one with the slots slightly angled with respect to the element axis. This slight angle is used to increase the slot coupling coefficients. The element consists of an array of six groups of slots. Each group of slots consists of three slots spaced 120 degrees apart around the circumference of the outer conductor. The groups of three slots each are linearly spaced one-half wavelength apart along the array axis. Alternate groups are angled alternately with respect to the element axis. This is necessary because the ridges on the center conductor reverse pitch every half-wavelength. The reason for the pitch reversal is to excite each group of slots in the proper phase with respect to the adjacent group to result in a broadside array. The empirically determined characteristic impedance of the ridged section of the element is approximate 13 ohms.

Since the characteristic impedance of the element section is 13 ohms and this is fed from a 50-ohm line, it was necessary to develop an impedance transformer. Considerable effort was devoted to transformer design techniques. A Tchebyscheff-type transformer with four steps was developed for the array under investigation.

A preliminary pattern was taken by using a triple stub tuner to match the element load. The patterns resulting were quite close to the desired patterns. At present a broadband impedance matching device for the element is being developed. This impedance matching device will most likely be two short sleeves on the center conductor near the impedance transformer on the input side.

STRUCTURE

During this report period the fabrication of the spacecraft structure assembly was completed (Figure 3-23). Electronic units were installed in preparation for the electronics performance demonstration.

Design work during the month included brackets for storage battery installation (which permits flexibility of location, for center of gravity and dynamic balance control). Space envelopes for the antenna electronics package and the apogee motor were completed. Motor tolerances and balance requirements were established, consistent with the spacecraft flight parameters (see Section 6). The dummy apogee motor fabrication is nearing completion. The motor case will be shipped to JPL for loading with inert propellant. Effort was initiated on the integration of the Marquardt vernier control system design into the spacecraft. Several unresolved problem areas exist, regarding space, load paths, and temperatures.

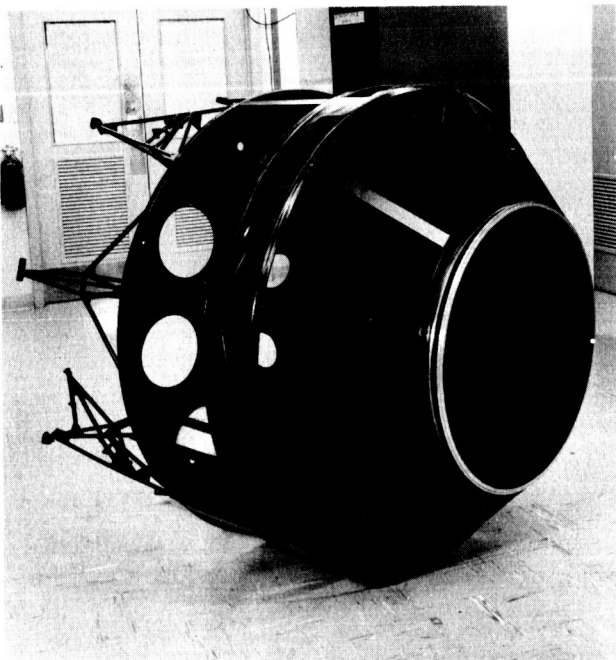


Figure 4-23a. Spacecraft Structure
Rear Quarter View

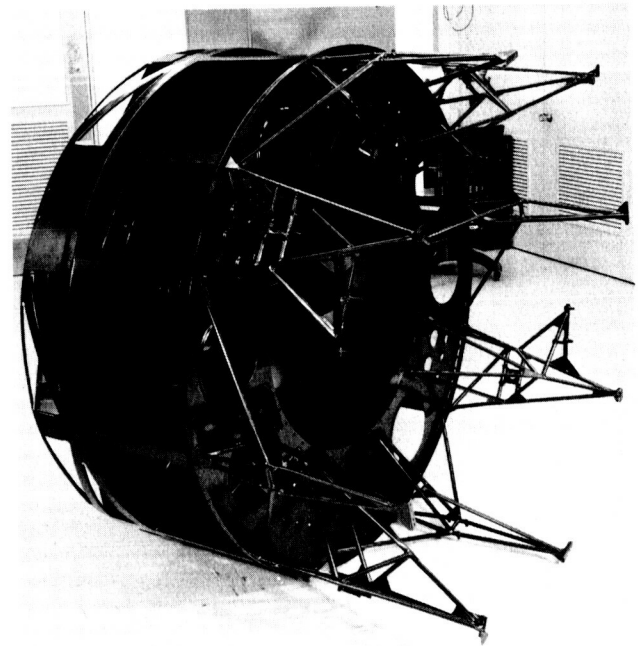


Figure 4-23b. Spacecraft Structure
Forward Quarter View

TABLE 3-2. SYNCOM II ESTIMATED WEIGHT STATUS
Solid-Propellant Configuration - Spacecraft

Subsystem	Δ Weight*	Weight, pounds	ϕ **		θ ***	
Electronics	-13.1	130.0	0.208		0.086	
Wire harness		19.9	0.032		0.013	
Power supply		105.5	0.169		0.069	
Controls		48.2	0.077		0.032	
Propulsion		122.2	0.196		0.081	
Structure	+ 6.0	138.3	0.222		0.091	
Miscellaneous	+ 6.6	60.1	0.096		0.040	
Item		Weight, pounds	z - z	I_{z-z}	I_{x-x}	R/P
Final orbit condition		(624.2)	23.5	57.2	45.4	1.26
N ₂ pressurization		3.0				
N ₂ H ₃ - CH ₃ fuel		53.5				
N ₂ O ₄ oxidizer		85.0				
Total at apogee burnout		(765.7)	23.5	71.0	52.3	1.36
Apogee motor propellant		752.3				
Total payload at separation		(1518.0)	24.7	85.7	67.2	1.28

* Change in subsystem weight since last report

** Ratio of subsystem weight to final orbit condition weight.

*** Ratio of subsystem weight to total payload at separation.

A center structure subassembly, with a 3/8-inch-thick aft bulkhead added for support, is being fabricated for use by Marquardt in testing their engineering model of the control system.

Structural Analyses

The T-1 vibration test plan has been completed (see Section 6). Development vibration tests have been completed on three additional solar panels as a continuation of the program delineated in the Advanced Syncom January monthly report. The test panel has been further modified to improve its response at the qualification levels, and it is currently being tested with solar cell covers, wiring, and electronics installed. The weight of the solar cells and cover glasses is simulated by using overweight cell covers. The panel selected for further testing is a modification of configuration "B", 0.25 inch thick without an internal stiffener. The results of the complete test series will be published subsequently.

Use of the GPS analog computer to study the 10 mass dynamic model has been precluded in favor of a digital computer solution for the axial and lateral vibration models. Computer input is being prepared, and results will be presented during the next report period.

Weight Summary, Flight Spacecraft

The latest weight data for the flight spacecraft configuration is shown in Table 3-2. An error in the apogee motor center-of-gravity location occurred in the Monthly Progress Report for January 1963 which resulted in higher roll-to-pitch moments of inertia than should have been shown. However, the design concept has since been altered to relocate the apogee motor 1.05 inches aft. This movement reduces the distance between motor and spacecraft centers of gravity and subsequently increases the roll-to-pitch moment-of-inertia ratios to the levels shown in the table.

Weight changes since the last weight statement are as follows:

Power Supply Subsystem

Batteries - Transfer of structural weight to structure subsystem	-11.3 pounds
Solar panels - New estimate	- 1.8 pounds

Structure Subsystem

Motor mount pads - Revised estimate	- 2.6 pounds
Battery supports - Transfer weight from power supply subsystem (net reduction estimated to be 1.0 pound)	+10.3 pounds

Miscellaneous Subsystem

Ballast - Increase to maintain maximum spacecraft weight of 1518 pounds + 6.6 pounds

Apogee motor propellant - JPL estimate + 0.5 pound

HANDLING AND WEIGHT AND BALANCE EQUIPMENT

A special spin test fixture for the performance of tests on a spinning spacecraft was fabricated and is being utilized. To obtain a more quiet operation, the hydraulic transmission was replaced by a "V" belt drive arrangement. Figure 3-24 shows the general view of the fixture. Figure 3-25a shows the spacecraft mounted. Figure 3-25b shows the spacecraft spinning.

The mobile assembly for final assembly and test purposes is being fabricated and completion is expected on schedule.

The hoisting sling has been constructed and is now available for use.

Two segment clamp assemblies, consisting of four segments each, were delivered.

The motor-charging special mandrel is now undergoing fabrication. When completed, the mandrel will be used by JPL in charging the motor with propellant. An accessory motor stand is also undergoing on-schedule fabrication.

The fixture to permit machining of apogee motor mounting pads is being fabricated.

The dynamic test fixtures have been designed and fabrication has been initiated.

HOT GAS REACTION JET CONTROL SUBSYSTEM

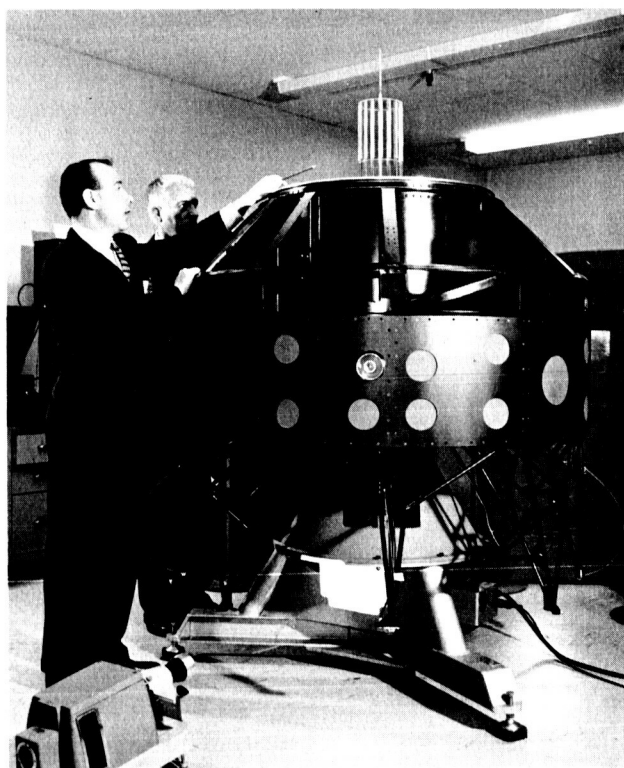
Marquardt Status

Authorization to proceed on the Syncom II reaction control system contract was given to Marquardt on 6 February 1963. Contractual items which have been received from Marquardt include a PERT diagram and a development plan for Phase I of the program. The PERT diagram was rejected because of lack of sufficient detail to control the program. Recommendations for minor modifications to the test plan are being made to Marquardt.

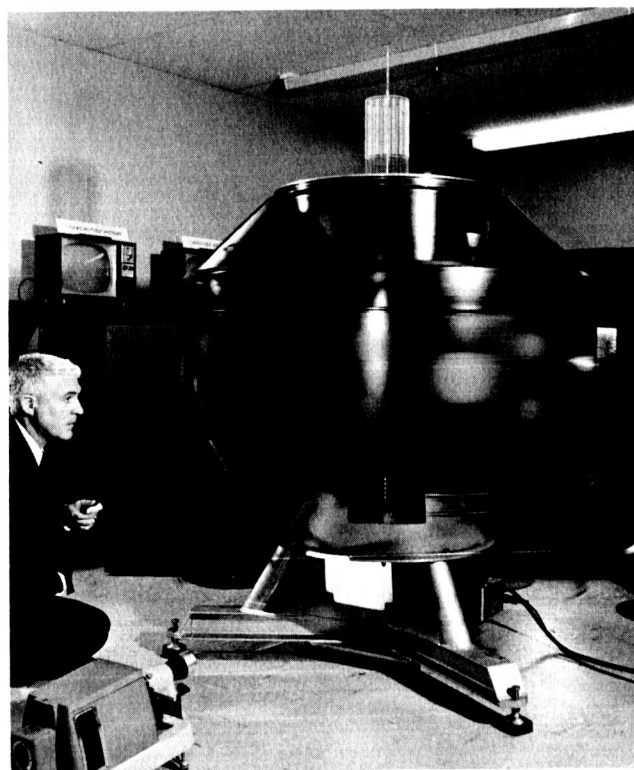
A meeting with Hughes and Marquardt was conducted to better define the swivel mount requirements for the axial engine. The analyses and designs developed by Hughes were given to Marquardt. An addendum to the Hughes Procurement Specification, defining specific swivel requirements, is being prepared.



Figure 3-24. Spin Test Fixture



a) Stationary



b) Spinning

Figure 3-25. Syncom II Spaceframe
Mounted on the Spin Test Fixture

The first development test of a thrust chamber assembly is 2 weeks behind the original schedule. The slippage is largely due to manufacturing delays. Multiple-shift shop operation is expected to regain the loss in schedule. The first firing of the thrust chamber is now expected to occur the third week of March.

Marquardt's instrumentation methods and capabilities were reviewed by representatives of NASA and Hughes and were generally acceptable.

Spin-Speed Control Mechanism (Figure 3-26)

During the report period primary effort on the spin-speed control mechanism consisted of viscous-bellow-damper development. Two types of tests were conducted:

- 1) Measurement of damping force versus frequency of input ($\pm 1/2$ degree amplitude.) (cf. Figure 3-37, January 1963 Advanced Syncom NASA Progress Report.)
- 2) Measurement of spin-speed mechanism damping characteristics both with and without a model damper installed, using an initial condition on position as the input.

Results indicated that:

- 1) Further analysis of bellows for the application is required. (The use of a welded plate bellows is under investigation.)
- 2) Detailed attention to the geometry of the damper application to the spin-speed control is required. (A layout of a modified damper is in process.)

It is planned to construct and test the modified damper in greater detail, in order to:

- 1) Estimate importance of parameters such as amplitude and temperature on damper operation.
- 2) Vibration test spin-speed control mechanism.
- 3) Centrifuge test spin-speed control mechanism.

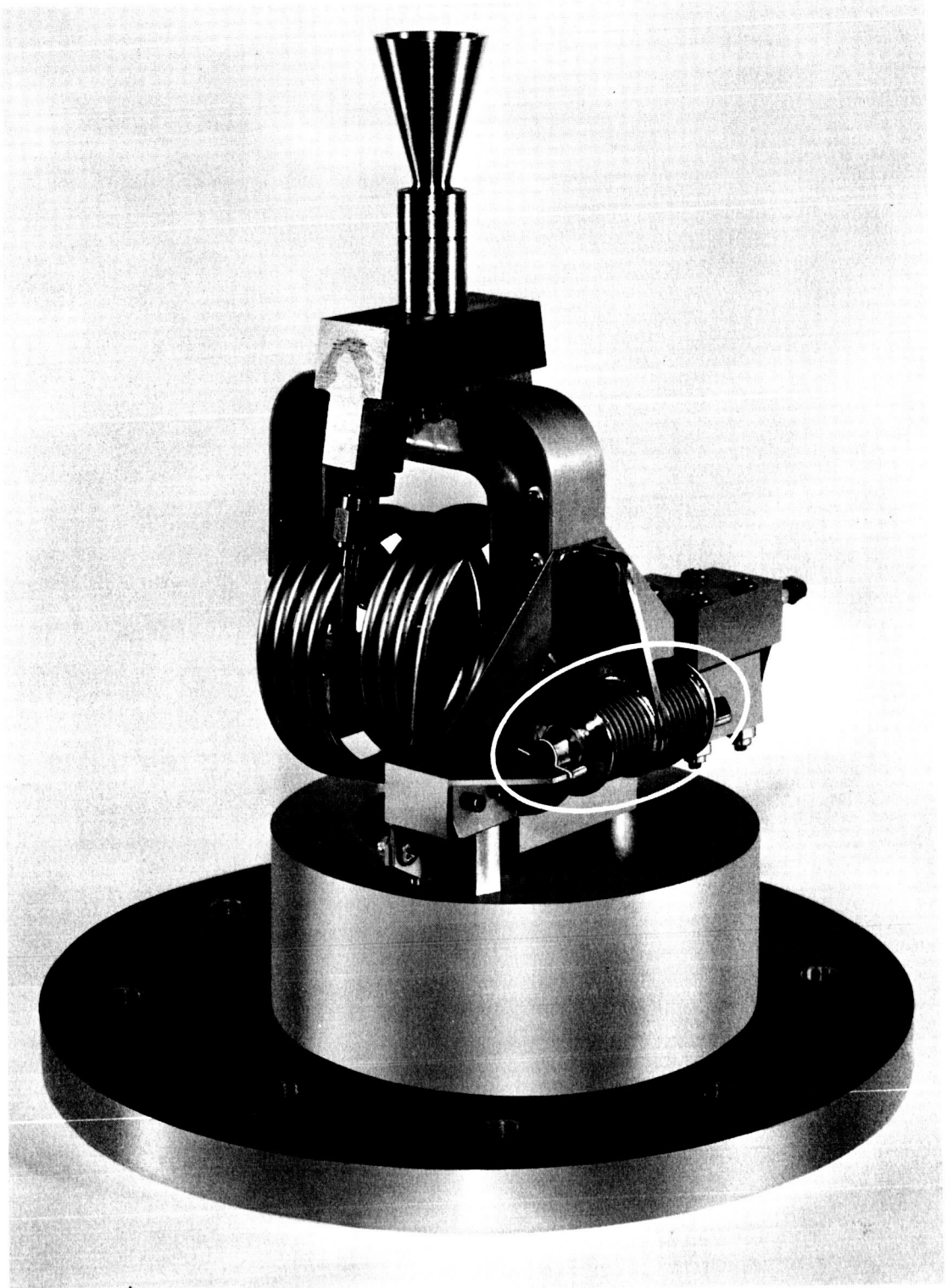


Figure 3-26. Spin Speed Control Mechanism
with Bellows Damper

APOGEE ENGINE LIAISON

The solid-propellant apogee engine for Syncom II is under development by the Jet Propulsion Laboratory for NASA. The engine, a scale-up of the Syncom I engine, consists of: 1) a 410 stainless steel case; 2) a composite molded nozzle assembly containing a ZTA graphite throat insert; 3) case insulation; 4) a case-banded polyurethane-type propellant; and 5) a pyrotechnic-type igniter.

JPL estimated the following weights for a vehicle boost capability of 1518 pounds:

Propellant	752.3
Inerts	<u>122.2</u>
Total engine weight	874.5 pounds

Agreement has been reached between NASA, Hughes, and JPL on engine performance and alignment requirements. JPL has initiated final design of engine components and tooling and has submitted a complete program plan to NASA.

Eight engines of the final configuration will be subjected to qualification testing. The eight-engine program is less than the Hughes' recommended minimum of 14 tests.

The dummy engine, to be used in structural testing of the spacecraft, will be available for test on 25 March 1963. The Hughes components will be shipped to JPL on 8 March which will permit JPL to load the engine with inert propellant prior to 18 March, the planned date for movement of the JPL loading facility to the Edwards Air Force Base site.

4. NEW TECHNOLOGY

There were no items of new technology reported during the report period.

5. PROJECT REFERENCE REPORTS

- Master Index, Syncom II Spacecraft, Flight Model 475000-100
Revision A, dated 5 February 1963
Revision B, dated 7 February 1963
Revision C, dated 21 February 1963
- Lotta, J. G., "Syncom II Weight Status," IDC 2243.11/265,
6 February 1963.
- Engineering Procedures Manual, Project Bulletin 7-17.1,
"Advanced Syncom Project - Engineering Data," 4 February 1963.
- Lotta, J. G., "HSX-302 T-1 Weight Status, Syncom II,"
IDC 2243.11/273, 15 February 1963.
- Brennan, R. A., "Syncom II Telemetry Reliability,"
IDC 2207.1/6, 15 February 1963.
- Rubin, P. A., "Review of RELAY Test Stations, "
IDC dated 26 February 1963.
- Culver, J. S., "Syncom II Apogee Motor Tolerances,"
IDC 2243.30/636, 27 February 1963.
- Meyer, J. C., "Syncom II Quality Control Information,"
IDC 2280.05/269, 28 February 1963.
- Letter Report, "Study of 4Gc and 6Gc Multiplexers for Syncom II,"
Purchase Order No. 4-753000-FF 31-1, 28 February 1963.
- Advanced Syncom, "Demonstration Plan," SSD 3114-B,
February 1963.

6. ATTACHMENTS

ATTACHMENT 1. SYNCOM II ENGINEERING MODEL VIBRATION TEST PLAN

Introduction

The structural test program for Syncom II* includes a vibration test of the engineering model. The vibration test will demonstrate the structural adequacy of the spacecraft at the qualification levels defined by NASA and will establish test levels for component qualifications.**

The engineering model represents the 1518-pound flight version of Syncom II. The structure will be vibrated from the Agena interface at launch weight and from the apogee motor attachments with the motor removed.

Test Program

The test is to consist of sinusoidal frequency sweeps at two input levels for each direction of excitation and shaker application. Random excitation will not be employed. Table 6-1 gives the run sequence. Figure 6-1 defines the excitation axes.

The qualification test inputs referred to in Table 6-1 are:

All axes, log sweep at 2 octaves/min, 4.3-minute duration

5 to 15 cps	1/4 inch double amplitude
15 to 250 cps	3.0 g 0 to peak
250 to 400 cps	5.0 g 0 to peak
400 to 2000 cps	7.5 g 0 to peak

* Syncom II Initial Project Development Plan, Volume I, SSD 23802.

** R. J. Oedy, "NASA-GSFC Engineering Design Tests for Atlas-Agena B and Thor-Agena B Payloads, " 1DC 2241.3/200, 26 June 1962.

TABLE 6-1. RUN SCHEDULE

Run	Input Location	Excitation Axis	Input Level
1	Agena interface	3	1/4 - 1/2 g
2	Agena interface	3	Qualification
3	Agena interface	1	1/4 - 1/2 g
4	Agena interface	1	Qualification
5	Agena interface	2	Qualification
6	Apogee motor mountings	1	1/4 - 1/2 g
7	Apogee motor mountings	1	Qualification
8	Apogee motor mountings	2	Qualification
9*	Apogee motor mountings	2	1/4 - 1/2 g
10	Apogee motor mountings	3	1/4 - 1/2 g
11	Apogee motor mountings	3	Qualification

* Slide table investigation.

A single electromagnetic shaker will excite the structure through suitable adapters. The thrust tube adapter design, which duplicates the Agena interface geometry, requires that the phased array antenna be removed. This adapter is to be attached to the thrust tube with a simulated Marman clamp and to the shaker or slide table with bolts, using the complete existing Ling 249 hole pattern.

For the second configuration an apogee motor adapter is to be located within the thrust tube and will duplicate the JPL motor attachments. The base of this adapter will consist of a circular plate drilled to match the complete Ling 249 hole pattern. The antenna electronics and associated structure are to be removed when this adapter is in use.

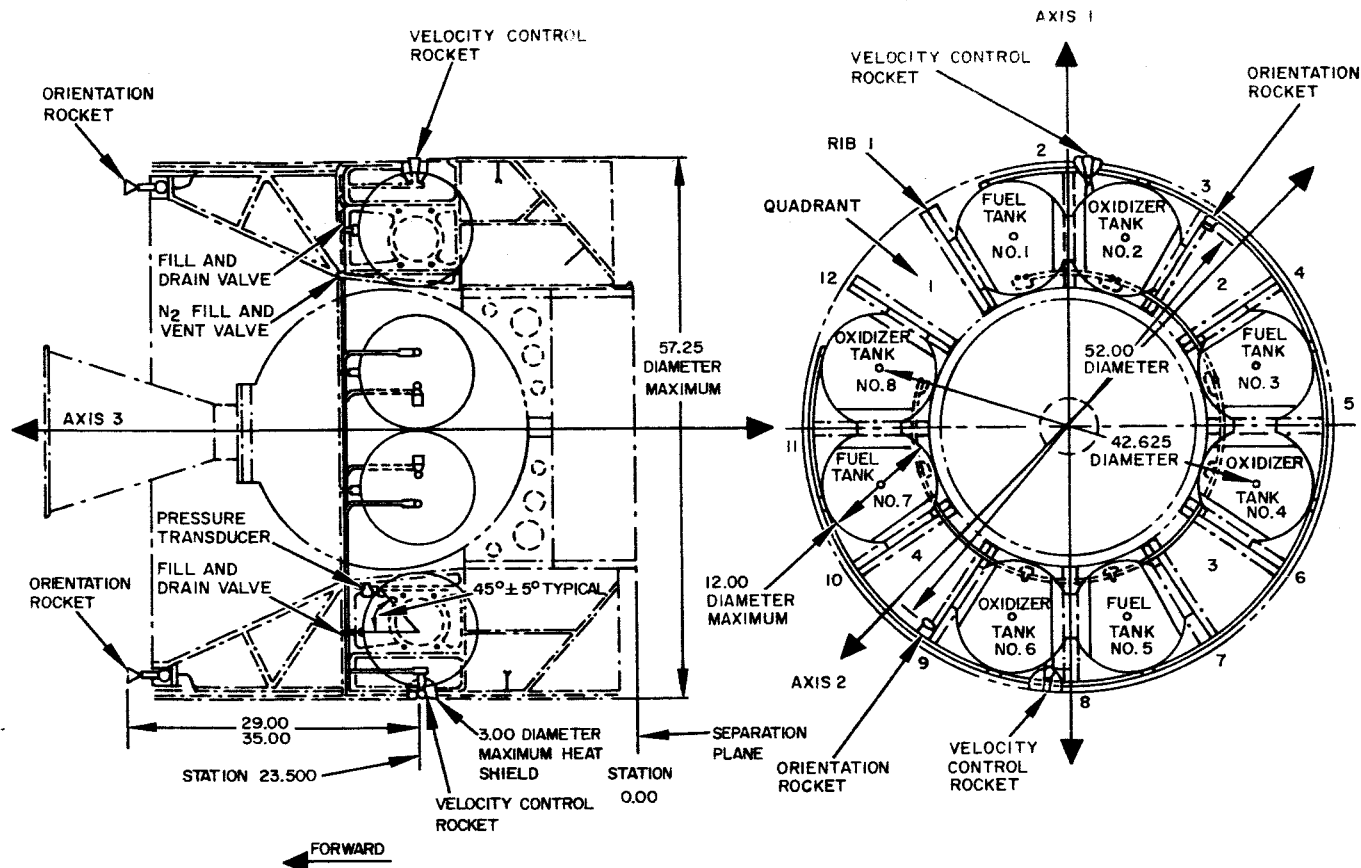


Figure 6-1. Syncom II General Arrangement

Instrumentation

The instrumentation will consist of 35 crystal accelerometers and 24 strain gage circuits. Phenolic accelerometer mounting blocks will be installed as shown in Table 6-2. Full bridge strain gage circuits will be located as shown in Table 6-3.

Data Acquisition

Accelerometer data will be recorded on two oscillographs having flat frequency response from 5 to 2000 cps. If additional tape recorders or multiplexing are available, they should be used instead of oscillograph recording.

Magnetic tape recordings are to be made of 13 selected accelerometer channels during qualification testing. The accelerometers to be recorded during each test run are given in Table 6-4. Strain gage data will be recorded on a separate, direct print recorder at slow speed during runs 2, 4, 5, 7, 8, and 11.

TABLE 6-2. ACCELEROMETER BLOCK LOCATIONS

Block	Location	Orientation
1	Truss over ribs 3 and 4, sun sensor platform	Along axis 2
2	Truss over ribs 12 and 1, sun sensor platform	Along axis 2
3	Truss over ribs 3 and 4, orientation rocket platform	Along axis 2
4	Forward bulkhead, flight termination timer	Along axis 2
5	Top of apogee motor case	Along axis 1
6	Top of bipropellant tank No. 6	Along axis 1
7	Top of bipropellant tank No. 7	Along axis 1
8	Top of bipropellant tank No. 8	Along axis 1
9	Quadrant 4 electronics, center of panel A	Along axis 2
10	Quadrant 4 electronics, center of panel B	Along axis 2
11	Quadrant 4 electronics, center of panel C	Along axis 2
12	Quadrant 1 electronics, center of panel A	Along axis 2
13	Quadrant 1 electronics, center of panel B	Along axis 2
14	Quadrant 1 electronics, center of panel C	Along axis 2
15	Velocity control rocket mount	Along axis 1
16	Apogee motor mount No. 5	Along axis 1
17	Apogee motor mount No. 8	Along axis 1
18	Rib 5, station 18, radius 27	Along axis 1
19	Rib 5, station 18, radius 15.5	Along axis 1
20	Rib 5, station 3, radius 15.5	Along axis 1
21	Rib 8, station 18, radius 27	Along axis 1
22	Rib 8, station 18, radius 15.5	Along axis 1
23	Rib 8, station 3, radius 15.5	Along axis 1
24	Antenna electronics, center of structure	Along axis 2
25	Upper solar panel attachment above rib 8	Along axis 1
26	Upper solar panel attachment between ribs 9 and 10	Along axis 2
27	Lower solar panel attachment between ribs 9 and 10	Along axis 2
28	Upper battery pack - above radial centerline - tank No. 6	Along axis 1
29	Lower battery pack - below radial centerline - tank No. 6	Along axis 1
30	Input - to be located	
31	Input - to be located	
32	Input - to be located	
33	Input - to be located	
34	Input - to be located	
35	Input - to be located	

TABLE 6-3. STRAIN GAGE BRIDGE LOCATIONS

Bridge	Location	Orientation
1	Thrust tube at station 3.5, rib 2	Fore and aft
2	Thrust tube at station 3.5, rib 5	Fore and aft
3	Thrust tube at station 3.5, rib 8	Fore and aft
4	Thrust tube at station 3.5, rib 11	Fore and aft
5	Upper flange of rib 2 at thrust tube	Radial
6	Lower flange of rib 2 at thrust tube	Radial
7	Upper flange of rib 11 at thrust tube	Radial
8	Lower flange of rib 11 at thrust tube	Radial
9	Tank mounting panel 2, inner stiffener	Fore and aft
10	Tank mounting panel 2, outer stiffener	Fore and aft
11	Tank mounting panel 11, inner stiffener	Fore and aft
12	Tank mounting panel 11, outer stiffener	Fore and aft
13	Truss	To be located
14	Truss	To be located
15	Truss	To be located
16	Truss	To be located
17	Tank mounting panel	To be located
18	Tank mounting panel	To be located
19	Tank mounting panel	To be located
20	Tank mounting panel	To be located
21	Rib web	To be located
22	Rib web	To be located
23	Rib web	To be located
24	Rib web	To be located

TABLE 6-4. ACCELEROMETER LOCATIONS

Run Number*	Block Number	Accelerometer Orientation	Run Number	Block Number	Accelerometer Orientation	Run Number	Block Number	Accelerometer Orientation
1, 2, 10, 11, (axis 3)	2	Axis 3	3, 4, 6, 7 (axis 1)	1	Axis 2	5, 8 (axis 2)	1	Axis 2
	3	Axis 3		3	Axis 2		2	Axis 2
	4	Axis 3		4	Axis 2		3	Axis 2
	5	Axis 3		5	Axis 1		4	Axis 2
	6	Axis 3		6	Axis 1		7	Perpendicular to 1
	7	Axis 3		6	Axis 3		8	Perpendicular to 1
	10	Axis 3		7	Axis 1		8	Perpendicular to 1
	13	Axis 3		8	Perpendicular to 1		8	Axis 3
	15	Axis 3		10	Axis 2		9	Axis 2
	16	Axis 3		13	Axis 3		10	Axis 2
	17	Axis 3		15	Axis 1		11	Axis 2
	18	Axis 3		16	Axis 1		12	Axis 2
	19	Axis 3		17	Axis 1		13	Axis 2
	20	Axis 3		18	Axis 1		14	Axis 2
	21	Axis 3		19	Axis 1		15	Axis 1
	22	Axis 3		20	Axis 1		16	Axis 1
	23	Axis 3		21	Axis 1		17	Axis 1
	24	Axis 3		21	Axis 3		18	Axis 1
	25	Axis 3		22	Axis 1		18	Axis 3
	28	Axis 3		23	Axis 1		19	Axis 1
	29	Axis 3		24	Axis 3		20	Axis 1
	30	Axis 3		25	Axis 1		21	Axis 1
	31	Axis 3		26	Axis 2		24	Axis 2
	32	Axis 3		27	Axis 2		24	Axis 3
	1	Axis 2		28	Axis 1		25	Axis 1
	6	Axis 1		29	Axis 1		26	Axis 2
	7	Axis 1		30	Axis 1		27	Axis 2
	9	Axis 2		31	Axis 1		28	Axis 1
	12	Axis 2		32	Axis 1		29	Axis 1
	16	Axis 1		5	Axis 3		5	Axis 3
	18	Perpendicular to 1		17	Axis 3		21	Axis 3
	21	Axis 1			Axis 3		30	Axis 3
	25	Axis 1					31	Axis 3
	26	Axis 2					32	Axis 3
	27	Axis 2						
	28	Axis 1						
	29	Axis 1						
	30	Axis 1						
	31	Axis 2						
	32	Axis 2						

* Accelerometers for Run No. 9 (the table investigation) will be positioned just prior to testing.

ATTACHMENT 2. SYNCOM II APOGEE MOTOR TOLERANCES

The limits on Syncom II apogee motor balance and nozzle alignment are defined by the effect on spacecraft flight dynamics of the combined motor and structure tolerances and balancing limits. An attempt has been made to apportion the total allowable tolerance spread in an equitable and realistic manner, taking account of customary machining practice and feasible limits on balancing techniques. Some flexibility can be permitted in the limits assigned the apogee motor; that is, a tradeoff among nozzle eccentricity, nozzle alignment, and dynamic and static balance allowances could be made.

The increase in spin rate during apogee motor burn, due to conservation of angular momentum of the propellant, has been ignored in this exercise, which makes the results slightly conservative. Independent variables have been combined by root sum squares, to define the 3σ conditions.

Calculations reported in the Advanced Syncom January Progress Report show that the spacecraft can tolerate a 3σ pitch torque of approximately 50 lb-ft average during apogee motor burn. This limit is defined by:

- 1) Maximum acceptable spacecraft attitude change
- 2) Allowable error in incremental velocity vector
- 3) Maximum nutation angle

Further, the rotation of the principal axis after burnout is limited to 0.2 degree (3.5 milliradians) 3σ value, due to:

- 1) Loss in effectiveness of the nutation dampers
- 2) Errors in the sun sensor readings

Two other limits--the change in spin rate due to a skewed thrust vector and the cg offset after burnout--proved to be very large compared to the preceding factors and thus were not controlling.

The calculations were based on an assumed time-thrust curve for the apogee motor (Figure 6-2). If the actual design curve is substantially different from that assumed, these limits will no longer apply.

The computations show that the requisite conditions will be met with the following tolerances:

- 1) Motor seat eccentricity to spacecraft centerline = 0.010 (includes effect of clearance between motor ring and motor seat).
- 2) Motor seat tilt with respect to spacecraft centerline = 0.010 inch in 28-inch diameter.
- 3) Spacecraft is balanced without bipropellants or apogee motor to 0.005 inch maximum cg offset, and 0.12 degree (2 milli-

- radians) maximum dynamic unbalance.
- 4) Motor nozzle passes through the motor mounting ring within 0.030 inch of the ring centerline.
 - 5) Motor nozzle centerline is perpendicular to the mounting ring within 0.001 inch per inch.
 - 6) The dynamic and static balance of the motor case, before loading, shall be as limited by curve A, Figure 6-3. The dynamic and static balance of the loaded motor shall be as limited by curve C, Figure 6-3.

Calculations for two extreme and two intermediate conditions of apogee motor balance (see Figure 6-3), are given below. Average torques for the four cases (Table 6-5) are shown to be 37.5, 39.0, 44.8, and 53.0 lb-ft. The final rotation of the principal axis for the four cases is 2.2, 2.4, 2.7, and 3.3 milliradians.

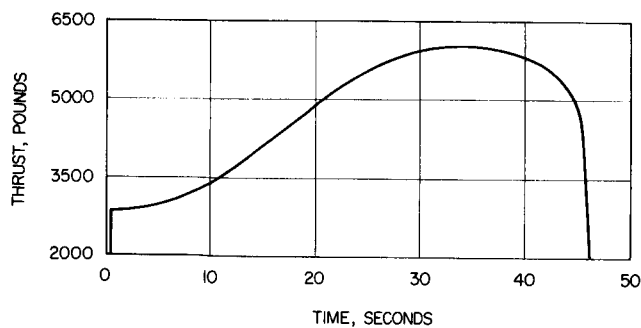


Figure 6-2. Estimated Thrust-Time Curve for Syncom II Apogee Motor

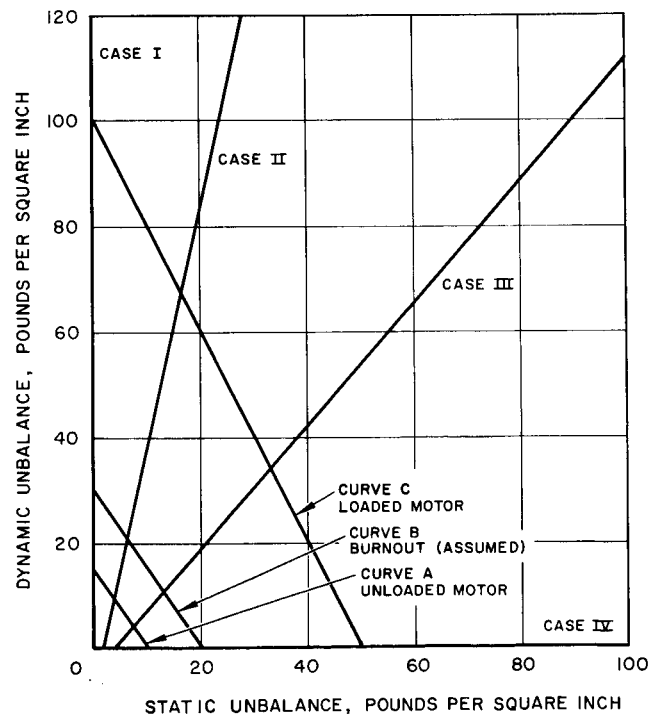


Figure 6-3. Maximum Sum of Static and Dynamic Unbalance in Syncom II Apogee Motor

TABLE 6-5. APOGEE MOTOR BALANCE CALCULATIONS

Time, seconds	Motor Dynamic Unbalance, I_{xx} lb-in ²	Motor Static Unbalance, I_{xx} lb-in	Motor Weight, WM pounds	Satellite Weight, WS lb	Motor CG, inches	Satellite CG, inches	CG-CGZ inches	Satellite CG Shift due to I_{xx} $D = \frac{I_{xx}}{WS}$	Satellite I_{xx} lb-in ²	Satellite $I_{xx'}$ lb-in ²	Satellite $I_{xx'} - I_{xx}$	Thrust, pounds	Satellite Dynamics Unbalance due to $I_{xx'}$ $I_{xx'}$ Z	Satellite Spin Axis Tilt due to $I_{xx'}$ ϕ	Satellite Spin Axis Tilt due to I_{xz} μ	Thrust Offset Armature Moment δ [0.029 + D]	Thrust Angle, Ω	RSS $[b + K]$	Torque $\frac{[b + K]}{12}$ lb-ft	Final Tilt of Principal Axis, RSS $[\psi + \phi + \mu]$ Radians	
CASE I																					
0	100	0	880	1518	27.7	25.2	2.5	0	396600	319050	77550	2850	0	0	0.0013	0.029	0.0028	0.101	0.105	24.9	
10	89	0	765	1403			4.5	0	389200	311650	77550	3400	0	0	0.0011	0.029	0.0027	0.097	0.101	28.6	
20	72	0	615	1253			6.0	0	370200	292100	78100	4850	0	0	0.0009	0.029	0.0026	0.094	0.098	39.6	
30	53	0	415	1053			7.3	0	352600	273600	79150	5950	0	0	0.0007	0.029	0.0025	0.090	0.094	46.6	
40	36	0	215	853			9.0	0	339000	259100	79900	5700	0	0	0.0005	0.029	0.0025	0.090	0.094	44.7	
45	30	0	120	758	33.6	23.5	10.1	0	328600	247750	80850	4700	0	0	0.0004	0.029	0.0024	0.087	0.092	36.1	
CASE II																					
0	67	17						0.011					42.5	0.0005	0.0009	0.031	0.0026	0.094	0.099	23.5	
10	59	16						0.011					72.1	0.0009	0.0008	0.031	0.0027	0.094	0.102	28.9	
20	48	13						0.010					78.0	0.0010	0.0006	0.030	0.0027	0.097	0.101	40.8	
30	35	10						0.009					73.0	0.0009	0.0004	0.030	0.0026	0.094	0.099	49.1	
40	24	8						0.009					72.0	0.0009	0.0003	0.030	0.0026	0.094	0.099	47.0	
45	20	7						0.009					70.8	0.0009	0.0002	0.030	0.0026	0.094	0.099	38.8	
CASE III																					
0	33	33						0.022					82.5	0.0011	0.0004	0.036	0.0027	0.097	0.103	24.4	
10	30	31						0.022					139.5	0.0018	0.0004	0.036	0.0031	0.112	0.117	33.2	
20	24	25						0.020					150.0	0.0019	0.0003	0.035	0.0031	0.112	0.117	47.3	
30	18	19						0.018					138.8	0.0018	0.0002	0.034	0.0030	0.108	0.113	56.0	
40	12	15						0.018					135.0	0.0017	0.0002	0.034	0.0030	0.108	0.113	53.6	
45	10	13						0.017					131.5	0.0016	0.0001	0.033	0.0029	0.104	0.109	42.7	
CASE IV																					
0	0	50						0.033					125.0	0.0016	0	0.044	0.0029	0.104	0.113	26.8	
10	0	47						0.033					211.5	0.0027	0	0.044	0.0036	0.130	0.137	38.8	
20	0	38						0.030					228.0	0.0029	0	0.041	0.0038	0.130	0.143	57.8	
30	0	29						0.027					212.0	0.0027	0	0.039	0.0036	0.130	0.136	67.5	
40	0	23						0.027					207.0	0.0026	0	0.039	0.0036	0.130	0.136	64.6	
45	0	20						0.026					202.0	0.0025	0	0.038	0.0035	0.126	0.131	51.4	
Average 37.5																					
Average 39.0																					
Average 44.8																					
Average 53.0																					

Calculations

Assumptions

- 1) Addition of bipropellants to balanced spacecraft adds static unbalance of 9 lb-in maximum and dynamic unbalance of 9 lb-in² maximum.
- 2) Static and dynamic unbalance of burned out motor are twice those of the unloaded motor case.
- 3) Static and dynamic unbalance of the motor decay from loaded to burnout condition in proportion to propellant burned.
- 4) Motor cg shifts from loaded to burnout location in proportion to propellant burned.

Computations

In searching for the worst conditions, four cases were assumed (see Figure 6-3) for motor tolerances:

Case I: maximum permitted dynamic unbalance (no static unbalance)

Case IV: maximum permitted static unbalance (no dynamic unbalance)

Cases II and III: equally spaced between these extremes

Pitching torque is the sum of motor thrust times the offset between the cg and the thrust vector, plus the lateral component of the thrust times the effective moment arm from the component to the cg.

$$\text{Torque} = \text{RSS} [(\text{thrust} \times \text{offset}) + (\text{thrust} \times \text{length} \times \sin \text{thrust angle})]$$

For small angles, where $\sin \text{angle} = \text{angle}$,

$$\text{Torque} = \text{RSS thrust} [\text{offset} + \text{length} \times \text{thrust angle}]$$

$$\text{Torque} = \text{RSS } T[\delta + l\Omega] \quad (6-1)$$

$$\begin{aligned} \delta = \text{RSS} [& A \text{ (mislocation of nozzle on motor)} \\ & + B \text{ (eccentricity of motor installation)} \\ & + C \text{ (mislocation of spacecraft cg before installing} \\ & \text{motor)} \\ & + D \text{ (shift of spacecraft cg due to motor unbalance)}] \end{aligned}$$

$$\delta = \text{RSS} [A + B + C + D] \quad (6-2)$$

A = 0.030 at station 16.5 (Drawing No. X209749)

\cong 0.022 at station 25 (see Figure 6-4)

B = 0.010 (Drawing No. X209698)

C = 0.015 (from tolerance (3) and assumption (1))

From Equation 6-2,

$$\delta = \text{RSS} [0.022 + 0.010 + 0.015 + D]$$

$$\delta = \text{RSS} [0.029 + D] \quad (6-3)$$

l = effective length from cg to point of action of lateral component of thrust; by inspection and estimate, effective point assumed to be 8 inches from nozzle exit plane

$$l = 36 \text{ inches} \quad (6-4)$$

Ω = thrust angle

$$= \text{RSS} [\alpha \text{ (nozzle angle with respect to motor mounting ring)} \\ + \theta \text{ (motor seat angle with respect to spacecraft geometric)} \\ + \gamma \text{ (tilt of spacecraft principal axis before installing motor)} \\ + \phi \text{ (tilt of spacecraft principal axis due to motor static unbalance)} \\ + \mu \text{ (tilt of spacecraft principal axis due to motor dynamic unbalance)}]$$

$$\Omega = \text{RSS} [\alpha + \theta + \gamma + \phi + \mu] \quad (6-5)$$

$\alpha = 0.001 \text{ inch/inch}$

$\theta = 0.010 \text{ inch in 28 inches diameter}$

$\theta = 0.00036$

$\gamma = 0.0022 \text{ (from tolerance (3) and assumption (1))}$

$$\phi = \frac{I_{xx} \cdot Z}{I_z - I_x} \quad (6-6)$$

where

I_{xx} = static unbalance of motor

Z = distance between motor cg and spacecraft cg with motor installed

I_z = roll moment of inertia of spacecraft

I_x = pitch moment of inertia of spacecraft.

$$\mu = \frac{I_{xz}}{I_z - I_x} \quad (6-7)$$

where I_{xz} is dynamic unbalance of the motor.

From Equation 6-5,

$$\Omega = \text{RSS} [0.001 + 0.0036 + 0.0022 + \phi + \mu] \\ \Omega = \text{RSS} [0.0025 + \phi + \mu] \quad (6-8)$$

Then from Equation 6-1,

$$\text{Torque(lb-ft)} = \text{RSS} \frac{T[\delta + 36\Omega]}{12} \quad (6-9)$$

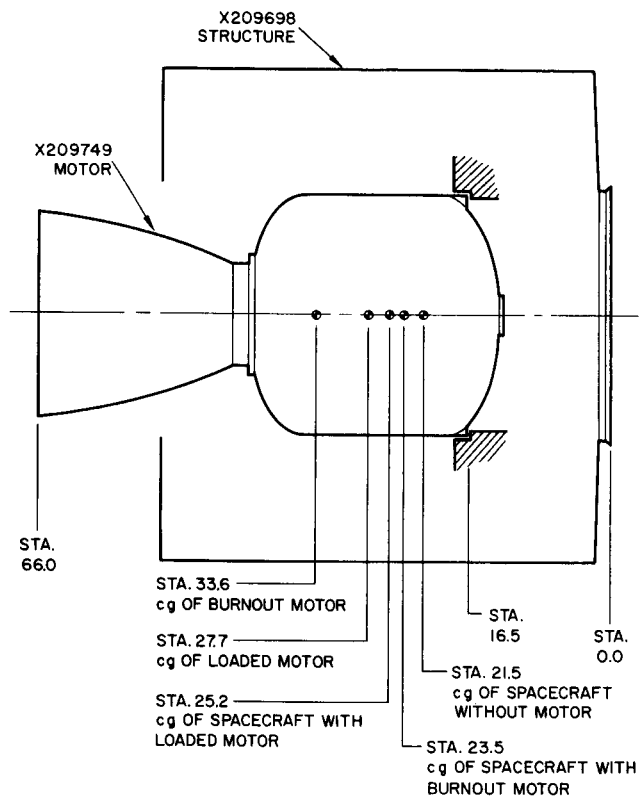


Figure 6-4. Motor and Spacecraft Geometry